

ABSTRACT

Title of Dissertation: SPACE-TIME BEHAVIOR OF MILLIMETER
WAVE CHANNEL AND DIRECTIONAL
MEDIUM ACCESS CONTROL

Behnam Neekzad
Doctor of Philosophy, 2008

Directed By: Professor John S. Baras
Department of Electrical and Computer
Engineering

An appropriate channel model is required to evaluate the performance of different physical (PHY) layer designs. However, there is no known space-time millimeter wave channel model that could benefit the use of directional antennas that is applicable in environments with lots of reflections such as residential or office. The millimeter wave signal strength is subject to temporal and spatial variations. The focus of the first part is the investigation of the characteristics of the millimeter wave propagation model. By analyzing measurement data of millimeter wave channels for indoor environments, space-time clusters are identified, and intercluster statistics for millimeter wave propagation are calculated. Correlation of the identified space-time clusters to the propagation environment is determined. In the second part, the effectiveness of the ray-tracing method in creating channel realizations in the intercluster and intracluster levels for millimeter wave indoor environments is

validated. In the third part, a protocol to establish an optimal directional link between two nodes equipped with directional antennas is presented. The correctness of the protocol for different scenarios is illustrated using a ray-tracing tool.

Then in the fourth part, a Directional MAC (D-MAC) for supporting millimeter wave technology exploiting directional antennas is presented. The D-MAC is compatible with the current IEEE 802.15 MAC of WPAN, and it has backward compatibility to support devices which are not equipped with directional antennas. Finally, a directional neighbor discovery algorithm is presented which does not require time synchronization or any location information of communicating nodes. This means two nodes equipped with directional antennas can discover and communicate with each other through an established directional link as part of the D-MAC.

SPACE-TIME BEHAVIOR OF MILLIMETER WAVE CHANNEL AND
DIRECTIONAL MEDIUM ACCESS CONTROL

By

Behnam Neekzad

Dissertation submitted to the Faculty of the Graduate School of the
University of Maryland, College Park, in partial fulfillment
of the requirements for the degree of
Doctor of Philosophy
2008

Advisory Committee:
Professor John S. Baras, Chair/Advisor
Professor Steven A. Tretter
Professor Adrian Papamarcou
Professor Richard La
Professor Guangming Zhang

© Copyright by
Behnam Neekzad
2008

Dedication

To my parents

and

To my wife

Acknowledgements

I would like to thank my advisor, Professor John S. Baras for his continuous guidance and support throughout my PhD studies. He encouraged and provided me the opportunity to work on and get familiar with a variety of subjects and research problems.

I would also like to thank Professors Steve A. Tretter, Adrian Papamarcou, Richard La, and Guangming Zhang for serving on my committee. I am also thankful to Professor Armand M. Makowski for serving on my PhD research proposal committee. I am especially grateful to Professor Steve A. Tretter for his support and friendship throughout my graduate studies.

I am especially indebted to my good friend and colleague, Dr. Kamran Seyrafian-pour, for his collaborative role in the pursuit and completion of this work. His tireless dedication, his many insightful comments, and his critical feedbacks on many of the projects proved invaluable in the development of the approaches presented in this thesis.

I would also like to thank the administrative staff of ISR and the ECE department notably, Maria Hoo, Althia Kirlew and Kimberly Edwards for their hard work and efficiency in shielding students from the countless administrative work. I am also grateful for the support of my research and my graduate studies through the NASA Grant NCC8235 with the University of Maryland at College Park.

Finally, I wish to express my sincere gratitude to my parents and my siblings for all they have done for me throughout my life, and to my wife, Nasim, for her encouragement, support and patience during my studies.

Table of Contents

Dedication	ii
List of Tables	vi
List of Figures	vii
Chapter 1: Overview	1
1.1 Our contributions	1
1.2 Thesis organization	2
Chapter 2: Space-time behavior of millimeter wave channels	4
2.1 Motivation	4
2.2 Large scale channel characterization	5
2.2.1 Path loss	5
2.2.2 Shadowing	6
2.3 Small scale channel characterization	7
2.4 Experiment setup	9
2.5 Space-time clean algorithm	14
2.6 Space-time kernel density estimation	18
2.6.1 Histogram	19
2.6.2 Developing space-time kernel density estimation	20
2.7 Cluster identification	21
2.8 Analysis	23
2.8.1 LOS residential environment	24
2.8.1 NLOS office environment	27
2.9 Conclusions	31
Chapter 3: Comparison of ray-tracing and millimeter wave channel sounding measurements	33
3.1 Ray-tracing	33
3.1.1 Motivation	33
3.1.2 WiSE	34
3.2 Comparison of ray-tracing results with measurement data	36
3.3 Space-time clusters and propagation environment correlation	38
3.4 Cluster energy	47
3.5 Conclusions	48
Chapter 4: Optimal directional link establishment	50
4.1 Motivation	50
4.2 Description and formulation of establishing an optimal directional link ...	51
4.3 A protocol to establish an optimal directional link between two nodes	53
4.4 Ray-tracing results	55

4.5	Conclusions.....	62
Chapter 5: Directional Medium Access Control (D-MAC), adapting the IEEE 802.15.3 MAC for millimeter wave technology..... 64		
5.1	Introduction.....	64
5.2	Overview of the current IEEE 502.15.3 MAC	66
5.2.1	Components of an 802.15.3 piconet	66
5.2.2	Dependent piconet	67
5.2.3	Starting a piconet	67
5.2.4	Structure of a superframe.....	68
5.2.5	Beacons	69
5.2.6	Contention Access Period (CAP).....	69
5.2.7	Channel Time Allocation Period (CTAP).....	71
5.3	Impact of millimeter wave technology on the current IEEE 802.15.3 MAC layer	72
5.4	Limitations of the IEEE 802.15.3 MAC to exploit directional antennas....	72
5.5	Directional Medium Access Control (D-MAC)	74
5.5.1	Basic D-MAC operations of a piconet of devices with directional antennas.....	75
5.5.2	Directional neighbor discovery.....	76
5.5.3	Integration of directional link establishment	80
5.5	Conclusions.....	82
Chapter 6: Summary of contributions and directions of future research		
6.1	Summary of contributions.....	83
6.2	Future research.....	84
Bibliography		
		86

List of Tables

Table (2-1): Measurement setup parameters

Table (2-2): Directional transmitter and receiver antennas

Table (2-3): Sample location and size of space-time clusters identified by space-time KDE

Table (2-4): Cluster coordinates for the residential environments

Table (2-5): Cluster coordinates for the office environments

Table (3-1): Matched cluster center's coordinates

List of Figures

Fig (2-1): 3D Representation of the received RF signal energy in the time and angle domains

Fig (2-2): 2D image of the clusters in the time and angle domains

Fig (2-3): The LOS scenario geometric layout

Fig (2-4): The NLOS scenario the geometric layout

Fig (2-5): Antenna patterns in the azimuth and elevation planes for: a) omni-directional antenna; and directional antennas with beamwidths of b) 60 degrees, c) 30 degrees and d) 15 degrees

Fig (2-6): The receiver antenna pattern in azimuth angles

Fig (2-7): Normalized PSF in the time and angle domains for the LOS measurement scenario

Fig (2-8): Space-time clusters identified after applying the space-time KDE

Fig (2-9): 2-D clusters in the residential LOS environment: a) omni; b) $\alpha=60^\circ$; c) $\alpha=30^\circ$; d) $\alpha=15^\circ$

Fig (2-10): Radio paths resulting to the clusters: a) 1, 2, 3; b) 4, 5; c) 6, 7

Fig (2-11): 2-D clusters in the office NLOS environment with TX omni-antenna

Fig (2-12): 2-D clusters in the office NLOS environment with directional TX antennas $\alpha=30^\circ$

Fig (3-1): A sample output of WiSE

Fig (3-2): Ray-tracing residential layout

Fig (3-3): Ray-tracing office layout

Fig (3-4): PDP of LOS arrival rays for TX: 360° and RX: 15° in the residential LOS scenario

Fig (3-5): PAP at arrival time of LOS rays for TX: 360° and RX: 15° in the residential LOS scenario

Fig (3-6): 2-D clusters identified from the measurement data in the residential LOS environment

Fig (3-7): 2-D clusters identified from ray-tracing data in the residential LOS environment

Fig (3-8): Cluster matching to the major arrival rays

Fig (3-9): Distribution of the relative angle of arrival rays

Fig (3-10): Distribution of the relative time of arrival rays

Fig (3-11): 2-D clusters identified from the experiment in the office NLOS environment with TX omni-antenna

Fig (3-12): 2-D clusters identified from the ray-tracing in the office NLOS environment with TX omni-antenna

Fig (3-13): Percentage of Normalized cluster energy for different antennas in the residential LOS environment

Fig (3-14): Percentage of Normalized cluster energy for different antennas In the office NLOS environment

Fig (4-1): Beam steering in array antennas

Fig (4-2): Ray-tracing layout

Fig (4-3): Beam pattern of a circular array with a) 8 elements b) 32 elements

Fig (4-4): Normalized RSS as a function of the direction of the transmitter/receiver's main lobes

Fig (4-5): α, β selected by the directional link establishment protocol for a LOS scenario

Fig (4-6): α, β selected by the directional link establishment algorithm for a NLOS scenario

Fig (4-7): RSS as a function of the direction of the transmitter/receiver's main lobes

Fig (4-8): Optimal directions of the transmitter/receiver's main lobes: a) Single reflected path; b) Double reflected paths

Fig (5-1): A Personal Area Network (PAN) with connected devices that might belong to a person

Fig (5-2): Elements of an 802.15.3 piconet

Fig (5-3): Parent and dependent piconets

Fig (5-4): Superframe structure

Fig (5-5): Unit Disk Graph model (UDG)

Fig (5-6): Basic D-MAC operation of piconet of DEVs equipped with directional antennas

Fig (5-7): Long Directional superframe (LD-superframe) for D-MAC

Fig (5-8): Short Directional superframe (SD-superframe) for D-MAC

Chapter 1: Overview

1.1 Our contributions

In the first part of this dissertation, by analyzing measurement data of millimeter wave channels for the indoor environment, space-time clusters are indentified. Intercluster statistics for millimeter wave propagation are calculated. Correlation of the identified space-time clusters to the propagation environment is determined. Knowledge of such spatial distribution of RF energy around the receiver in conjunction with directional antennas and appropriate signal processing algorithms can lead to systems that provide superior performance by taking advantage of clusters location and their corresponding characteristics.

In the second part, the effectiveness of ray-tracing in creating channel realizations in the intercluster and intracluster levels for millimeter wave indoor environments is validated. Ray-tracing can be an effective tool to predict millimeter wave propagation and especially location of the clusters around a receiver. Ray-tracing as a prediction tool can be very valuable when designing a system for a specific environment or to predict millimeter wave wireless channel characteristics.

In the third part, a protocol to establish an optimal directional link between two nodes equipped with directional antennas is presented. The correctness of the protocol for different scenarios is evaluated and illustrated using a ray-tracing tool. The established directional link achieves higher signal strength at the receiver; and therefore, a more reliable link can be expected.

In the forth part, a Directional Medium Access Control (D-MAC) which is compatible with the current IEEE 802.15 MAC of WPAN for millimeter wave technology exploiting directional antennas is given. The D-MAC can still support devices which are not equipped with directional antennas.

Finally, a directional neighbor discovery algorithm is presented which does not require time synchronization or any location information of communicating nodes. This means that two nodes equipped with directional antennas can discover and communicate with each other using the presented D-MAC.

1.2 Thesis organization

The thesis is organized as follows:

Chapter 2 discusses the space-time behavior of millimeter wave channels. The experimental setup is described, and a space-time clean algorithm to remove measurement and antenna effects is presented. Space-time kernel density estimation and cluster identification are described. The 2-D clustering phenomenon of millimeter wave propagation at indoor environments and the influence of geometry on this phenomenon are presented. Particularly, the effect of directional antennas with various beamwidths at the transmitter on the formation of such clusters is given.

In chapter 3, the influence of geometry on the clustering phenomenon of a millimeter wave channel through the use of a ray tracing tool is captured. It is shown that for indoor environments ray-tracing could be an effective tool to predict the location of the clusters around a receiver. Chapter 3 presents comparison of ray-tracing results with millimeter wave channel sounding measurements. The correlation

of space-time clusters and the propagation environment are described. Cluster energy is also determined.

In chapter 4, a protocol for establishing an optimal directional link between two nodes equipped with directional antennas is given. The underlying philosophy is to exploit the information in the spatial distribution of RF energy around both the transmitter and receiver, which results in better quality communication links. The proposed protocol outlines a methodology to obtain the directions, which the beam steering algorithms at the receiver and transmitter should use. The established directional link achieves higher signal strength at the receiver; and therefore, a more reliable link can be expected. Ray-tracing results to validate the correctness of the protocol are presented.

In chapter 5, a D-MAC which is compatible with the current IEEE 802.15.3 MAC to support millimeter wave technology exploiting directional antennas is presented. The basic functionality and structure of the current IEEE 802.15.3 MAC are reviewed. The impacting factors of millimeter wave technology on MAC are discussed. In addition, limitations of the current IEEE 802.15.3 MAC to support directional antennas are presented. Then, the new designed structure and basic operations of D-MAC are described, and modified frames of D-MAC are introduced. The directional neighbor discovery algorithm based on directional link establishment protocol is given. It is based on actual antenna patterns, and it does not require prior arrangements between communicating nodes. Integration of the directional link establishment algorithm into the D-MAC, and backward compatibility of the D-MAC with the current IEEE 802.15.3 MAC are discussed.

Chapter 2: Space-time behavior of millimeter wave channels

2.1 Motivation

Millimeter wave technology is becoming increasingly important in many military and commercial applications. Remote sensing, radio astronomy, passive imaging, radar and high data rate communication are among these applications. To establish a high data rate communication link between two nodes, acceptable Signal to Noise Ratio (SNR) at the receiver is required. However, due to the high propagation path loss and signal attenuation that is associated with the millimeter wave signal, it is extremely valuable to have knowledge of how millimeter wave signals propagate in the environment. Such information along with appropriate antenna technology could enable a system to maximize the quality of the received signal and therefore, achieve higher throughput.

Indoor environments create challenging multipath propagation scenarios with significant time and angular spread. Joint temporal-angular clustering phenomena have been observed at frequencies commonly used in wireless networks and 2-D statistical channel models have been proposed based on such phenomena [1], [2]. However, at millimeter wave frequencies, and to the best of our knowledge, no reports have been made for such clustering behavior. The clustering of arrival rays can have a significant impact on channel capacity. Un-clustered models tend to overestimate the capacity if the multipath components are indeed clustered [10].

Considering the angular (i.e. spatial) aspects of indoor channels is extremely important for systems employing multiple antennas. Millimeter wave wireless communication systems can greatly benefit from this knowledge as the physical size

of such array antennas makes them amenable to practical implementation. Knowledge of cluster locations is especially useful for such systems as it could be exploited by various spatial diversity combining or beamforming algorithms to enhance the system's performance.

The objectives of this study are the investigation of the 2-D clustering phenomenon of millimeter wave propagation (60 GHz) in indoor environments and particularly characterize the effect of directional antennas with various beamwidths at the transmitter on the formation of such clusters.

2.2 Large scale channel characterization

The large scale component is a result of distance-dependent propagation loss and attenuation due to large obstacles (i.e., shadow loss) such as walls, floors, ceilings, large furniture, etc. These large scale variations are observable over large distances (i.e., many meters), and are typically modeled as log-normal random variables for outdoor environments. In the following, we briefly introduce path loss and shadowing.

2.2.1 Path loss

The path loss is defined as the ratio of the received signal power to the transmit signal power and it is very important for link budget analysis. Unlike for narrowband systems, the path loss for wideband systems such as Ultra Wide Band (UWB) or millimeter wave is both distance and frequency dependent [12], [13]. In order to simplify the models, it is assumed that the frequency dependence of path loss is negligible and only the distance dependence of path loss is considered. The path loss as a function of distance is given by:

$$PL(d)[dB] = \overline{PL}(d)[dB] + X_{\sigma}[dB] \quad (2-1)$$

where \overline{PL} [dB] is the average path loss and X_{σ} is the shadowing fading, which will be described next. An example of the path loss model frequently used in the literature is:

$$PL(d)[dB] = 20 \log\left(\frac{4\pi d_0}{\lambda}\right) + 10.n.\log\left(\frac{d}{d_0}\right) \quad d \geq d_0 \quad (2-2)$$

where d_0 , λ and d denote the reference distance, wavelength and distance, respectively. The first component is free path loss at the reference distance and the second one is the path loss exponent at the relative distance. The path loss exponent n for millimeter-wave based measurements ranges from 1.2-2.0 for LOS and from 1.97-10 for NLOS, in various different indoor environments.

2.2.2 Shadowing

Due to the variation in the surrounding environments, the received power will be different from the mean value for a given distance. This phenomenon is called shadowing which causes the path loss variation about the mean value. Many measurement results reported in the millimeter-wave range have shown that the shadowing fading is log-normally distributed i.e. $X_{\sigma}[dB] = N(0, \sigma_L)$ where X_{σ} denotes a zero mean, Gaussian random variable in unit decibels with standard deviation σ_L , which has site specific value.

The shadowing parameters are calculated under the assumption that the channel is static and there is no movement of humans. In the presence of human

movement, measurement results show that the obstruction by humans can be significant and ranges from 18-36 dB [14], [15]. Furthermore, the duration of the shadowing effect is relatively long, up to several hundreds of milliseconds and this duration increases with the number of persons within the environment [14].

2.3 Small scale channel characterization

The small scale components are the result of constructive and destructive interference of multiple radio propagation paths (i.e., Multipaths) which arrive at the receiver with different propagation delays, strengths and phases [16], [23], [27]. Most of the data observed up to now, suggest a two-dimensional clustering phenomenon that takes place in millimeter wave indoor channels. Radio frequency energy that reaches the receiver travels via multiple paths. These paths seem to form clusters in angle and time. A sample 3D plot of the RF signal energy at the particular receiver

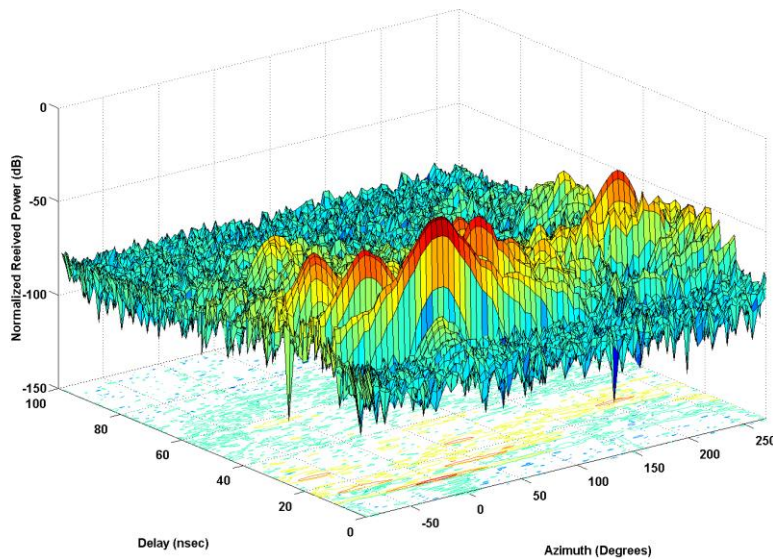


Fig (2-1): 3D Representation of the received RF signal energy in time and angle domains

position in an indoor environment is shown in Fig (2-1). Another useful way to represent this space-time clustering phenomenon is through a 2D image plot as shown in Fig (2-2). Axes in the plot represent the time and the azimuth angle of arrival rays.

A very popular channel model which explains the clustering phenomenon observed in the measurement data is based on the extension of the Saleh-Valenzuela (S-V) model, [8], to the angular domain (i.e. azimuth). The Channel Impulse Response (CIR) in complex baseband is given by

$$h(\tau, \phi) = \sum_{l=1}^L \sum_{k=1}^{K_l} \alpha_{k,l} \delta(\tau - T_l - \tau_{k,l}) \delta(\phi - \Theta_l - \omega_{k,l}) \quad (2-3)$$

where $\delta(\cdot)$ is the ‘‘Dirac’’ delta function, L is the total number of clusters and K_l is the total number of arrival rays within the l^{th} cluster. The scalars $a_{k,l}$, $t_{k,l}$ and $\omega_{k,l}$

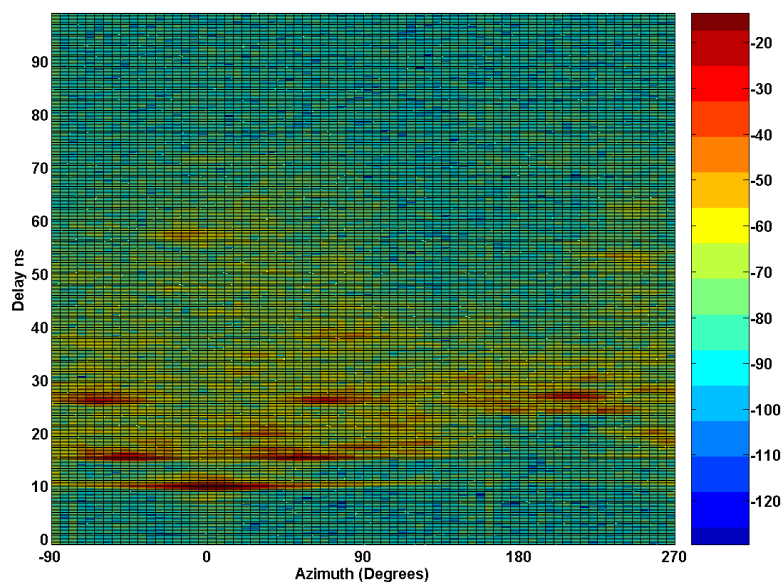


Fig (2-2): 2D image of the clusters in the time and angle domains

denote the complex amplitude, Time of Arrival (ToA) and azimuth Angle of Arrival (AoA) of the k^{th} ray of the l^{th} cluster. Similarly, the scalars T_l and Θ_l represent the ToA and AoA of the l^{th} cluster, which are defined as the ToA of the first arriving ray, and the mean of AoA of all arriving rays within the l^{th} cluster.

In reality, all of the parameters in (1-3) are randomly time-varying functions. However the variations are very small compared with the signaling rate and it is, therefore, reasonable to assume them to be time-invariant random variables. It is also important to note that each of the multipaths in (2-3) will experience distortions due to the frequency dependency of the scatterers [2], but this is not accounted for in our study due to lack of information.

The channel model relies on two classes of parameters, namely, intercluster and intracluster parameters which characterize the clusters and the arrival rays, respectively. From (2-3), $\{L, T_l, \Theta_l\}$ and $\{K_l, \tau_{k,l}, \omega_{k,l}, \alpha_{k,l}\}$ are classified as the intercluster and intracluster parameters, respectively.

2.4 Experiment setup

Measurement data for millimeter wave propagation (i.e. 57-64 GHz) are difficult to obtain. The difficulty is not only due to the cost of the required equipment but also to the manual labor that is needed to obtain many data points by repeating the experiments in different scenarios. In our analysis, we had access to the set of measurement data that has been obtained by the National Institute of Communication Technology (NICT) of Japan.

The measurement scenarios are done for two different environments: home and office. In the home scenario, the measurements are taken in an empty living

room, where the transmitter and receiver face-up each other so there is a Line Of Sight (LOS) between them. The room is without fixtures; the surface of side walls and ceiling are covered with wallpaper; the window is plane glass and the entrance door is wooden. Fig (2-3) shows a photo and geometric layout of the room. On the other hand, for the office scenario the measurements are taken in an office where No Line Of Sight (NLOS) between transmitter and receiver exists. The office room contains several desktop computers and desks; the room is made of steel walls, steel

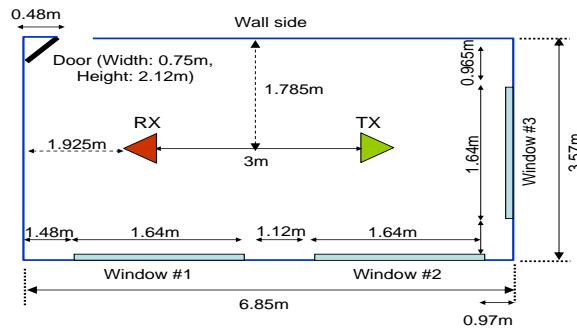


Fig (2-3): The LOS scenario geometric layout

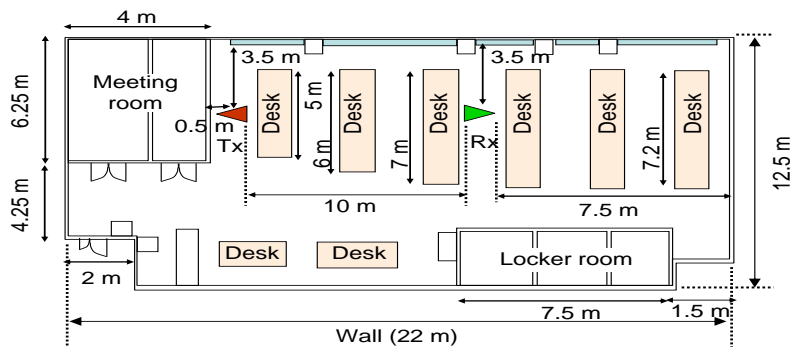


Fig (2-4): The NLOS scenario geometric layout

ceiling and steel floor; the plate glass windows are attached on the walls, the floor and the ceiling are covered with carpet and plaster board respectively. Fig (2-4) shows geometric layout of the office.

Using a Vector Network Analyzer model HP8510C, a frequency bandwidth of 3 GHz with center frequency of 62.5 GHz is scanned with steps of 7.5 and 3.75 MHz in LOS and NLOS scenarios respectively. For increasing accuracy and reducing possible errors, each stored data point is an average of 128 times of its measurement scenario. The table (2-1) represents the detail of measurement setup parameter values.

Table (2-1): Measurement setup parameters

Environment	Home (LOS)	Office (NLOS)
Center frequency	62.5 GHz	62.5 GHz
Bandwidth	3 GHz	3 GHz
Frequency steps	7.5 MHz	3.75 MHz
Number of frequency samples	401	801
Repeated times in average	128	128

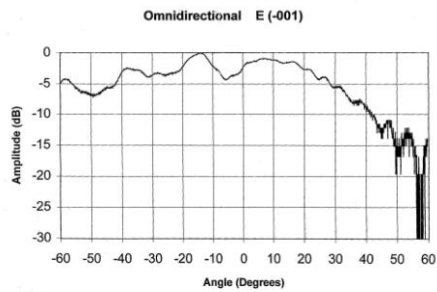
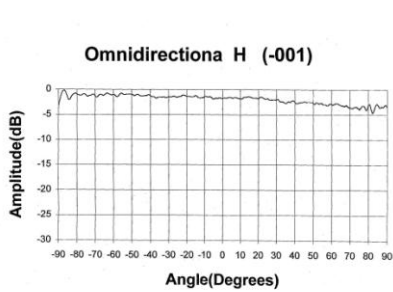
In all the measurement scenarios, the receiver antenna is directional with 3-dB beamwidth of azimuth angle equal to 15 degrees but the transmitter antenna is changed. In the LOS and NLOS scenarios, four and two different transmitter antennas are exploited to collect the experimental data. Omni and directional antennas with 3-dB beamwidths of azimuth angles equal to 360, 60, 30 and 15 degrees are utilized in the LOS scenario, while omni-directional 360 degrees and directional antenna with beamwidth of 30 degrees are employed in the NLOS scenario. The omni and

directional antennas have vertical polarization and are located at the height of 1.1 meters from the floor. The actual patterns of the different antenna gains in the azimuth and elevation planes are illustrated in Fig (2-5).

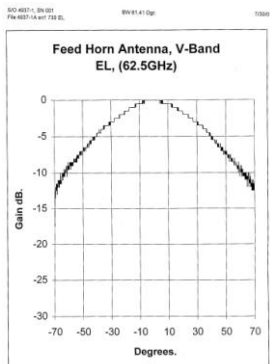
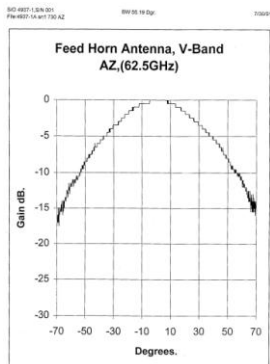
To measure the angular arrival rays for different utilized antenna pairs, the transmitter antenna is always kept fixed but the receiver antenna is rotated clockwise from 0 to 360 degrees with 5 degrees steps in the azimuth plane. The details of the transmitter and receiver antenna pairs and the rotation steps to collect measurement data are given in table (2-2).

Table (2-2): Directional transmitter and receiver antennas

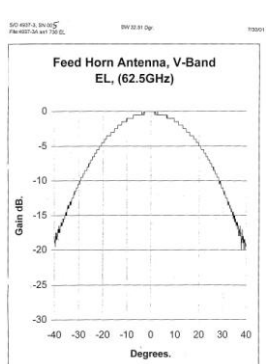
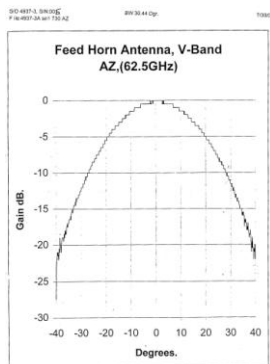
Scenario	Antenna Beamwidth		Rotation Angles [deg]
	Tx [deg]	Rx [deg]	
Home (LOS)	Omni	15	0,5,...,360
	60		
	30		
	15		
Office (NLOS)	Omni	15	0,5,...,360
	30		



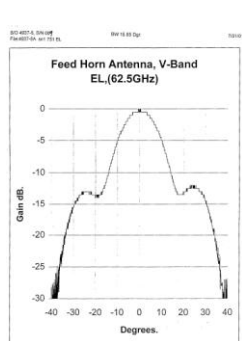
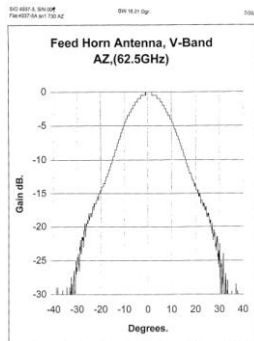
a)



b)



c)



d)

Fig (2-5): Antenna patterns for azimuth and elevation planes for: a) Omni-directional antenna; and directional antennas with beamwidths of b) 60 degrees, c) 30 degrees and d) 15 degrees

2.5 Space-time clean algorithm

Although diffuse and scattered multipath components are visible in the images of Fig (2-1) and Fig (2-2), most of the propagated energy is highly localized in space and time. The measured data at the receiver are affected by the transmitted pulse, rotation and beam pattern of the transmitter and receiver antennas. In other words, in the measurement scenarios, the rays arriving closely together, from the temporal or spatial point of views, are convolved. Particularly, considering the actual receiver's antenna pattern, illustrated in Fig (2-6), the individual multipath components are accumulated in the angular direction while the receiver antenna is turned on each 5 degrees step of the azimuth angles. We should note that the receiver's antenna pattern isn't a narrow beamwidth (i.e. pencil beamwidth), but it has a nominal 3-dB beamwidth of 15 degrees and it is greater than rotating angular steps in azimuth

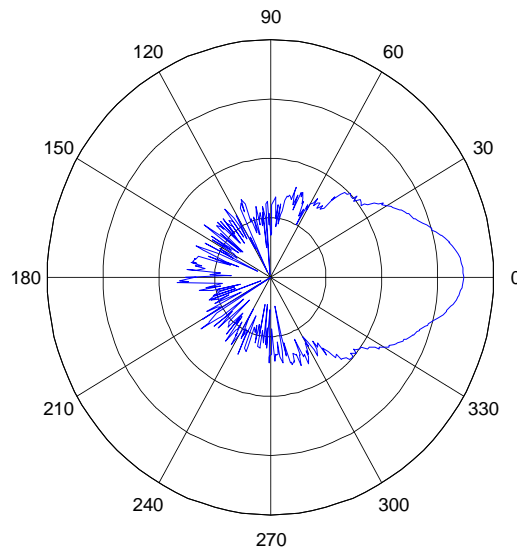


Fig (2-6): The receiver's antenna pattern in azimuth angles

(i.e. 5 degrees). So by pointing the main lobe of the antenna at any direction, not only the arrival rays at the pointing direction but also the multipath components of the neighbor angles are accumulated in the provided measured data.

The measured data are overlapped together and the original measured data set are a convolved version of arrival rays. The acquired data samples need to be off-line processed in order to statistically model the channel independently from the excitation signal and the transmitter and receiver antennas pattern. In order to restore the actual multipath components, the measured data should be deconvolved. In general the deconvolution process on real-life data is a tough problem and there is extensive literature on different applications (e.g. deblurring an image which is blurred by a moving object or removal of instrumental effects on measurement data). As such, the images shown in Fig (2-1) or Fig (2-2) can be modeled as a collection of point sources blurred by a point spread function (PSF) and corrupted by additive noise. This assumption reduces the problem of identifying exact times and angles of arrival for multipath components to a two dimensional (2-D) deconvolution process, which would normally be very difficult in the diffuse source or scattering case [1].

The PSF or ideal 2-D impulse response of the system was generated by using a band limited exciting signal (i.e. 3 GHz) and the receiver's antenna pattern. In other words, the PSF represents the case where the antennas are perfectly faced - aligned in LOS direction - and the excitement pulse is transmitted and received in a well-behaved environment, where reflections could be gated out (i.e. multipath-free environment).

The PSF in the LOS scenario is shown for a time range of 0 to 100 nsec in steps of .25 nsec and azimuth angles of 360 degrees with steps of 5 degrees. For example the resulting PSF in the LOS measurement scenario is shown in Fig (2-7). The sidelobes along the angular axis result from the beam pattern of the antenna, while the sidelobes in time result from the effects of windowing and pulse shaping. Although the sidelobes are present in both the spatial and temporal domains, it is seen that the spatial sidelobes are much stronger than the temporal ones, which causes more overlap on the measured arrival rays in the angular direction.

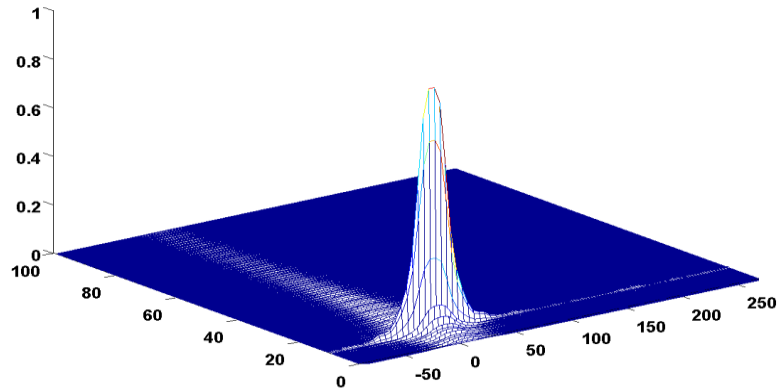


Fig (2-7): Normalized PSF in time and angle domains for the LOS measurement scenario

Because the point spread function is known with reasonable accuracy, the deconvolution problem lends itself well to the subtractive CLEAN algorithm [1]. The CLEAN algorithm was originally used for processing astronomical images, which are also often modeled as groups of point sources convolved with a blurring function. The CLEAN algorithm, introduced by [17], assumes that the radio sky can be represented by a number of point sources in an otherwise empty field of view.

Considering the measurement process and knowing the aforementioned PSF, we modified the CLEAN algorithm to fit the nature of the space-time channel data. Our clean algorithm is implemented in the following steps:

1. Normalize the original image, which is named dirty image (i.e. in the dirty image divide all the arrival ray strengths by the maximum one).
2. Find and store the strength, angular and temporal position of the peak ray (i.e., of the greatest absolute intensity) in the dirty image.
3. Shift the peak of the PSF according to the time and angle of the peak ray of the dirty image.
4. Update the dirty image by subtracting linearly in the time and circularly in the angular domain, the shifted PSF multiplied by a damping factor.
5. Go to step (2) unless any remaining peak in the updated dirty image is below some specified level. Otherwise save the remaining dirty image as residual.
6. Build abstract clean image by the stored rays from step (2).
7. Add the residual to the abstract clean image to build the actual cleaned image

The developed clean algorithm is essentially a recursive subtraction of the shifted PSF from the dirty image. The highest peak is found; its amplitude, time, and angle are stored; the PSF positioned to correspond with the maximum ray of the dirty image is built. Then a scaled copy of the shifted PSF is subtracted from the dirty image. This process is repeated on the residual image until a predetermined threshold (usually corresponding to the noise level) is reached. Also we should note that the angular nature of the data requires that the developed clean algorithm has to wrap

around in space, so this particular implementation has to take this into account by circular subtraction in angular domain, but this wouldn't be necessary for other applications.

2.6 Space-time kernel density estimation

The space-time clusters in the receiver location are contributed by arrival rays, which are strong enough and their intensities are higher than a noise level threshold. The arrival rays are 2-D random variables in time and angle. We are looking for a method to identify the space-time clusters and to measure the density of the arrival rays that contain an unknown number of the clusters with unidentified characteristics such as size or location. We developed and utilized a space-time Kernel Density Estimation (space-time KDE) method for this purpose. The space-time KDE procedure is preferred due to its robustness, simplicity and convenience to identify the space-time clusters and to predict the distribution of the arrival rays in the temporal and angular dimensions. Especially the space-time clusters become more obvious after applying the space-time KDE procedure to the data and the clusters can be easily identified by visual inspection. In the following, we first briefly introduce the general idea of nonparametric density estimation of a random variable data set. Then we explain the space-time Kernel Density Estimation (space-time KDE) algorithm.

In the data set collected by the measurement scenarios, we have time and angle of the strong arrival rays which are a realization of 2-D random variables (t_i, a_i) $i = 1, 2, \dots, N$. We want to estimate the 2-D probability density function (PDF) that represents these arrival rays. To study the behavior of these arrival rays, instead

of assuming a parametric model of some known distribution, such as a 2-D Gaussian distribution, with unknown expectation and variance and trying to find the associated parameters; we rather want to be as general as possible. This means we only assume that the density exists and is suitable smooth (e.g. differentiable). Then it is possible to estimate the unknown density function of the arrival rays.

2.6.1 Histogram

One way to estimate the unknown density of arrival rays is using a histogram [7]. By selecting an origin (t_0, a_0) and the bandwidths h_t and h_a for the temporal and angular dimensions, the space versus time plane is divided into equal size $h_t \times h_a$ rectangles. The histogram counts the number of rays falling into each rectangular area. Then in a 3-D plot of a histogram, the area of each bar is proportional to the number of arrival rays falling into the corresponding rectangle. The choices of origin, temporal and spatial bandwidths h_t and h_a are important; the 3-D plot of the histogram depends very much on these tuning parameters. In order to estimate the density of arrival rays with less dependency to fine tuning of the origin and bandwidths, we require a better estimator. In other words, to smooth out the contribution of each arrival ray over its local neighborhood and also to be independent of the width and end points of the rectangular area, we adapt a space-time Kernel Density Estimator (space-time KDE) algorithm which is independent of the origin selection.

2.6.2 Developing space-time kernel density estimation

Instead of choosing a rectangle weight function in the histogram estimator, we can select a 2-D kernel function $K(x, y)$ which is nonnegative and integrates to one for Kernel Density Estimation. The Kernel Density Estimation (KDE) is a nonparametric Probability Density Function (PDF) estimation approach that can be applied to a given set of measured data [7], [8]. KDE is a robust, simple and convenient method to estimate the PDF of a random variable given its sample realization. We have used the two dimensional version of this technique in order to estimate the temporal-angular distribution function of the ray arrivals at the receiver. Having this distribution function and using an appropriate threshold, all 2-D clusters (i.e. temporal-angular) can be easily identified. In other words if

$$K(x, y) > 0, \quad \int_{-\infty}^{+\infty} \int_{-\infty}^{+\infty} K(x, y) dx dy = 1, \quad (2-4)$$

then, the multivariate kernel estimation at time t and angle a , can be calculated as follow:

$$\hat{f}(t, a) = \frac{1}{Nh_t h_a} \sum_{i=1}^N K\left(\frac{(t, a) - (t_i, a_i)}{h_t h_a}\right) \quad (2-5)$$

where h_t and h_a are the temporal and angular bandwidths respectively. The (t_i, a_i) , $i = 1, 2, \dots, N$, comprise random variables of the arrival rays from some

unknown density $f(t, a)$. The positivity of the kernel function $K(x, y)$ guarantees a positive density estimate $\hat{f}(t, a)$. Typically, the kernel function $K(x, y)$ is chosen as a probability density. The smoothness of the density estimate $\hat{f}(t, a)$ is inherited from the smoothness of the kernel function: if the r^{th} derivative $K^r(x, y)$ exists for all (t, a) , then $\hat{f}^r(t, a)$ exists as well for all (t, a) , which can be easily verified using the chain rule for differentiation [6].

The kernel function is often selected to be a PDF that is symmetric both in time and angle [9]. In our study, we have used the 2-D *Normal* distribution to be the kernel function as written below:

$$K(x, y) = \frac{1}{2\pi} \exp\left(-\frac{1}{2}\|(x, y)\|^2\right). \quad (2-6)$$

Therefore, the Kernel Density Estimate of $f(t, a)$ will be:

$$\hat{f}(t, \theta) = \frac{1}{Nh_t h_\theta} \sum_{i=1}^N \frac{1}{2\pi} \exp\left(\frac{-\|(t, \theta) - (t_i, \theta_i)\|^2}{2h_t h_\theta}\right). \quad (2-7)$$

Using this approach, we have processed the time-angle impulse response of the channel obtained through both measurement and simulation.

2.7 Cluster identification

Different researchers have different definitions of a cluster [20], [21]. Here, we define a space-time cluster as an accumulation of arrival rays with similar ToAs and AoAs. The clustering of arrival rays can have a significant impact on channel

capacity. Unclustered models tend to overestimate the capacity if the multipath components are indeed clustered [10]. This implies that a more comprehensive characterization of the clustering and correlation properties is required.

After applying the space-time KDE algorithm, we can easily identify the space-time clusters; find their location, count and size in the temporal and angular domains. For illustration, Fig (2-8) shows a sample of identified space-time clusters.

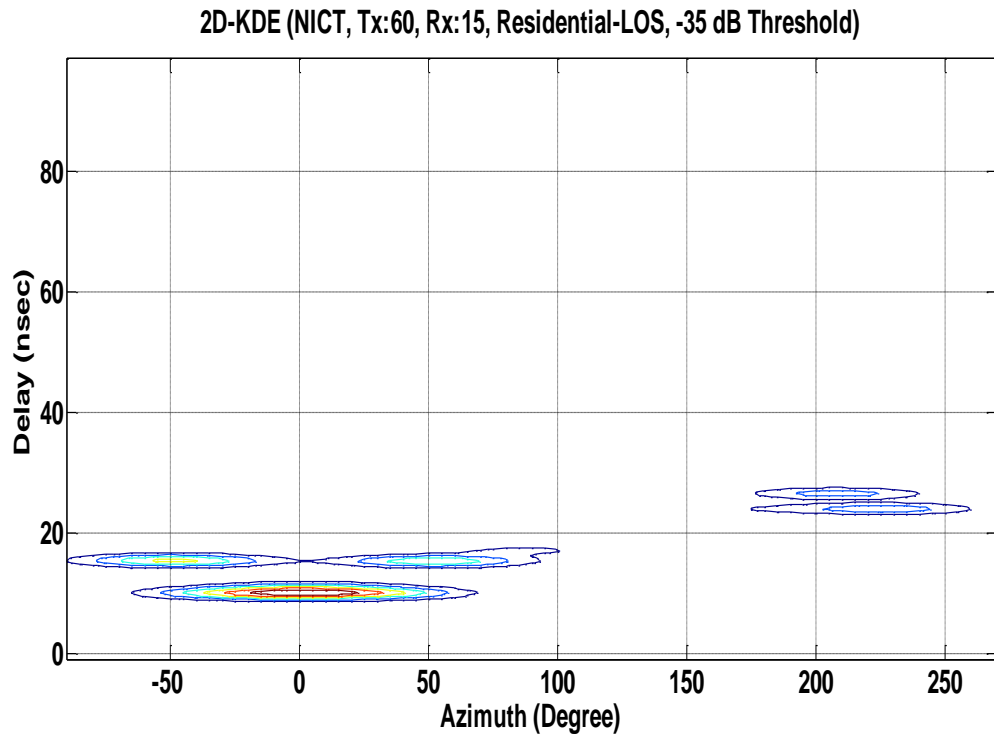


Fig (2-8): space-time clusters identified by the space-time KDE

The table (2-3) shows the number (I), mean angle (Θ_l) and arrival time (T_l) of the clusters. We investigate how these intercluster parameters of the millimeter wave channel change for the LOS and NLOS scenario. More over, we study the effects of transmitter and receiver antenna patterns on the intercluster parameters

Clearly, arrival rays into a cluster don't have equal power so we define the effective cluster angle as a weighted average of the angles of the arrival rays into the cluster.

Table (2-3): Sample location and size of space-time clusters identified by space-time KDE

Cluster #	Approximate Cluster Arrival Angle (Degrees)	Approximate Cluster Arrival Time (nsec)
l	Θ_l	T_l
1	0	10
2	-50	15.5
3	50	15.5
4	210	25.75

In other words, we first weight each arrival ray based on its power then find the average and define it as the effective cluster angle. If the receiver antenna points its antenna beamwidth to the effective cluster angle instead of the cluster angle, there would be a higher gain in the received signal.

2.8 Analysis

One dimensional temporal clustering phenomena have been observed in indoor channels and wideband statistical channel models have been proposed accordingly. Here, we also observe that arrivals come in few groups (i.e. clusters) scattered in different coordinates throughout the time-angle space. These 2-D clusters are identified by using the developed space-time KDE and an appropriate threshold representing the noise floor of the receiver.

2.8.1 LOS residential environment

Fig (2-9 a) displays the clusters obtained by processing the measurement data when an omni-directional antenna is used in the residential environment. A total of 7 clusters are observed in the channel data. The coordinates of these clusters are listed in Table 2-4. A cluster time (angle) coordinate is defined to be the median of the time (angle) of all arrival rays in that cluster.

Table (2-4): Cluster coordinates for the residential environments

Cluster #	Cluster Arrival Angle (Degrees)	Cluster Arrival Time (nsec)
1	0°	10
2	-50°	15.5
3	50°	15.5
4	-74°	25.75
5	74°	25.75
6, 7 (merged)	207.5 0°, 152.5 0°	25.75

A comprehensive geometric interpretation of these results can be provided by considering the main paths that the RF signal travels between the transmitter and receiver [19]. Each cluster formation is the result of a unique path between the transmitter and receiver. These paths which include direct LOS and various single-reflected and double-reflected signals have been graphically identified in Fig (2-10).

There are no clusters due to reflections from the walls behind the transmitter or receiver. This is because the transmitter and receiver are positioned at the same height and the measuring equipment (e.g. covered by electromagnetic absorbers in case of the transmitter) blocks the path of the reflected signal from either wall.

Similarly, Fig (2-9 b, c) and Fig (2-9 d) display the clusters obtained by processing the measurement data when directional antennas with beamwidths of 60, 30 and 15 degrees are used respectively in LOS scenarios (the residential environment). In these plots ' α ' represents the 3-dB beamwidth of the transmitting antenna. It is interesting to observe that as the beamwidth reduces, all clusters that occur due to paths outside the beamwidth of the antenna disappear. In other words, if the angle of departure of a path leading up to a cluster falls outside the beamwidth

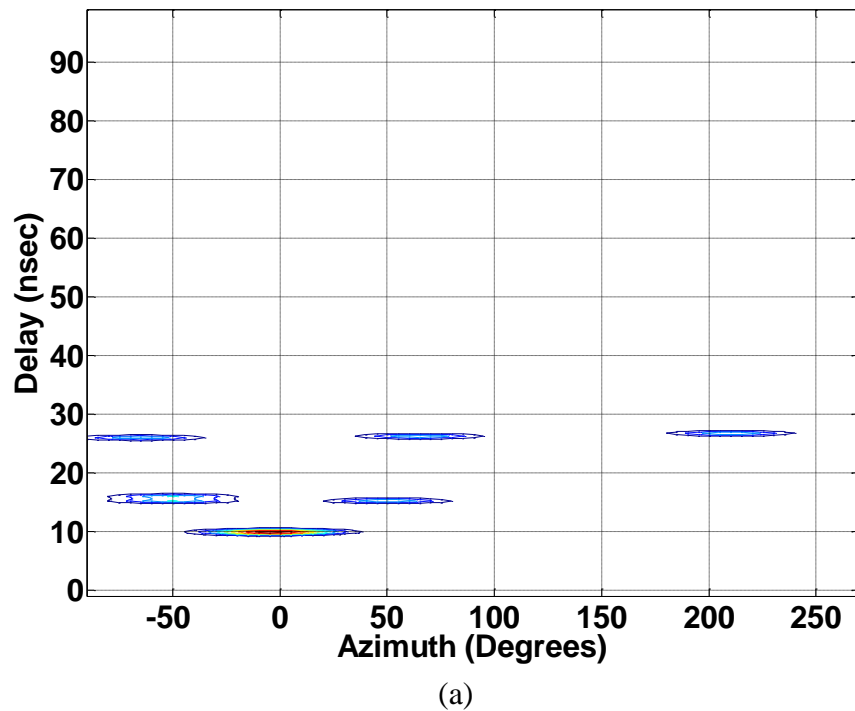
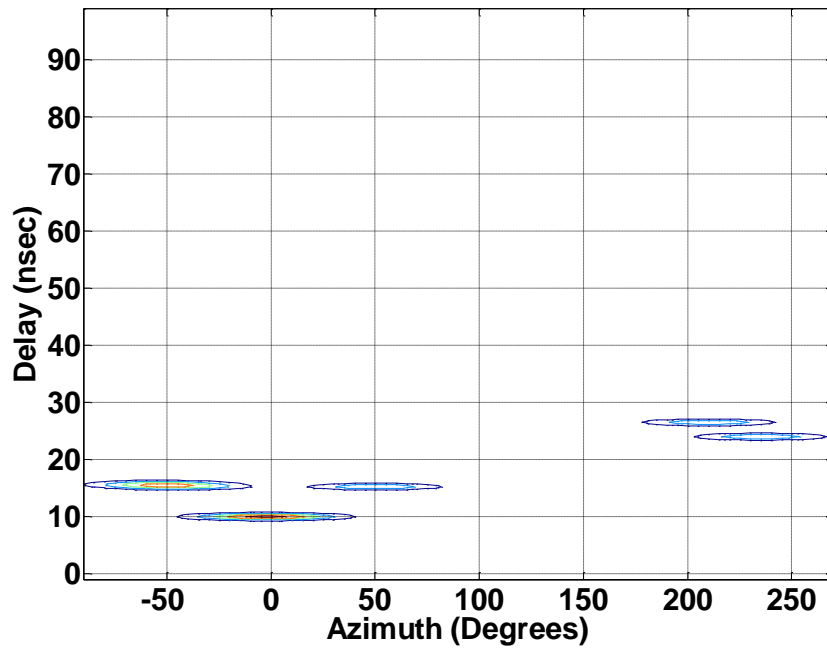
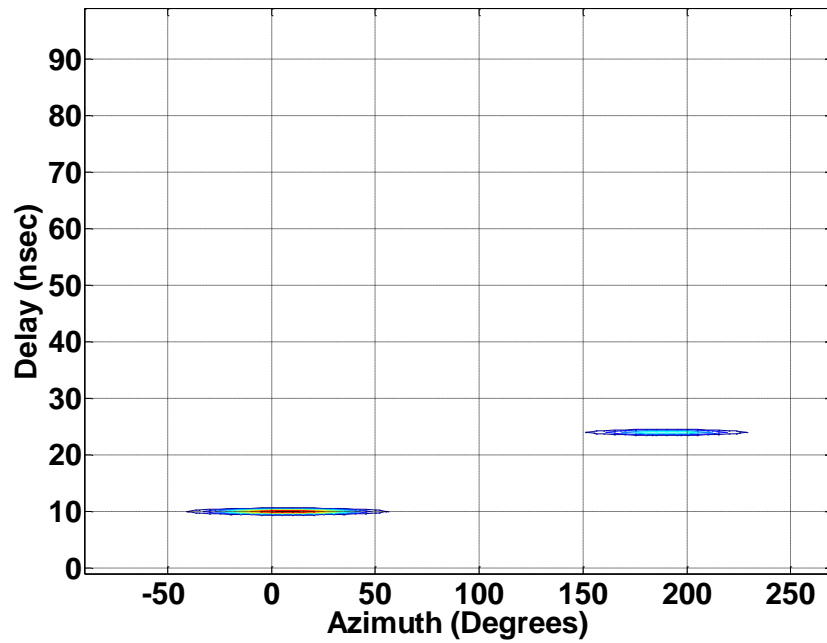


Fig (2-9 a): 2-D clusters in the residential LOS environment: a) Omni

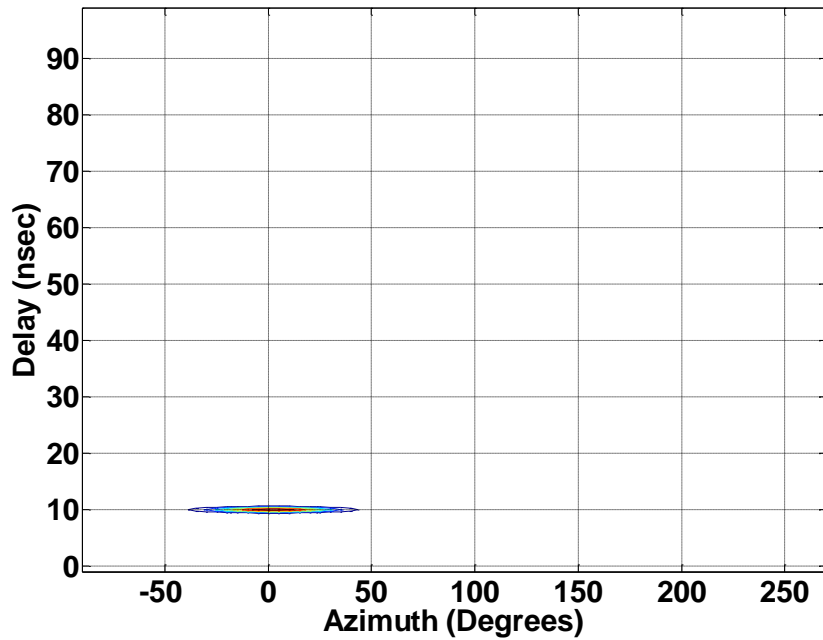


(b)



(c)

Fig (2-9 b, c): 2-D clusters in the residential LOS environment: b) $\alpha=60^\circ$ c) $\alpha=30^\circ$



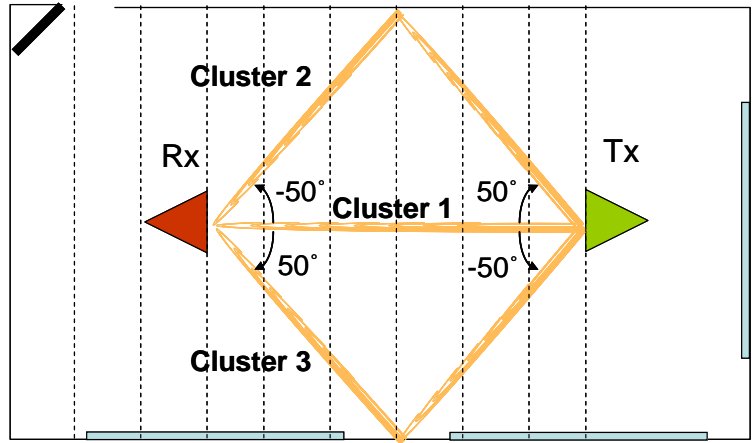
(d)

Fig (2-9 d): 2-D clusters in the residential LOS environment: d) $\alpha=15^\circ$

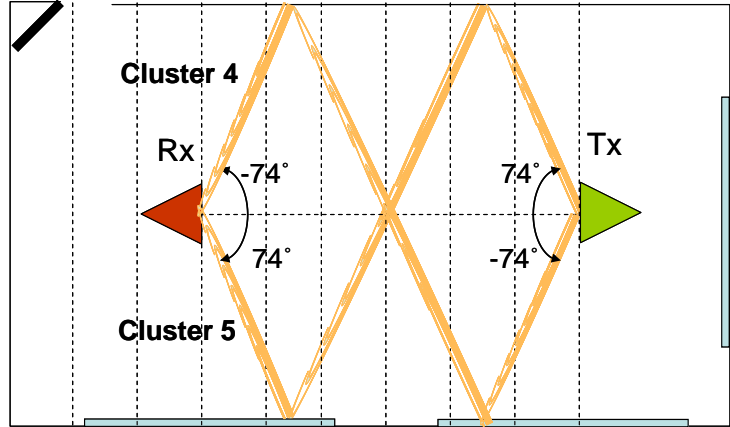
of the transmitter antenna, then the corresponding cluster will not be formed at the receiver. For $\alpha=15^\circ$, only the LOS cluster with minimal delay spread is observed. This is consistent with our expectation that as α gets smaller, channel behavior approaches an AWGN channel.

2.8.1 NLOS office environment

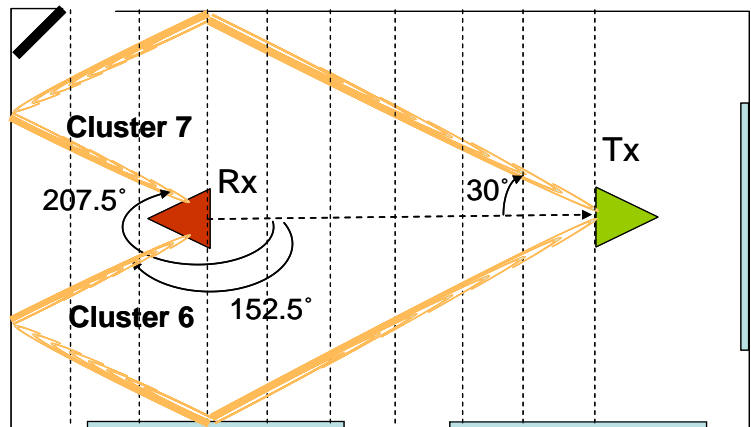
The data from the NLOS office environment was also processed for cluster identification. Fig (2-11) demonstrates the clusters that have been identified from the measured data. The scattering effect of the furniture and other office equipment in this environment causes some spreading in the shape of the clusters. For the omnidirectional case, a total of 4 clusters are observed in channel data that are the results of the LOS and single-reflected paths.



(a)



(b)



(c)

Fig (2-10): Radio paths resulting to clusters: a) 1, 2, 3; b) 4, 5; c) 6, 7

The coordinates of these clusters are listed in Table (2-5). The direct path between the transmitter and receiver, cluster 1, and the arrivals due to the reflection from the metal wall, cluster 2, have merged and formed a bigger cluster. The cluster 3, occurs because of the single reflection from the metal wall behind the receiver.

Table (2-5): Cluster coordinates for the office environments

Cluster #	Cluster Arrival Angle (Degrees)	Cluster Arrival Time (nsec)
1	0	37
2	-55	67.5
3	210	79
4	178	117.5

Looking at the time coordinates of some of these clusters, a mismatch is observed between the results and a geometric calculation based on the RF paths. A physical explanation for this discrepancy can be given by noticing the velocity change of RF waves as it goes through different materials that exist on its path between the transmitter and receiver [13]. In general, the exact coordinates, shape and size of the clusters depends on the details of the propagation environments; however, as seen here, the locations of the main clusters (i.e. high density) can be reasonably approximated by using information about the layout and locations of the transmitter-receiver pair.

The clusters in Fig (2-11) are due to the use of an omni-directional antenna at the transmitter. If a directional antenna is used instead, arrivals become more localized in

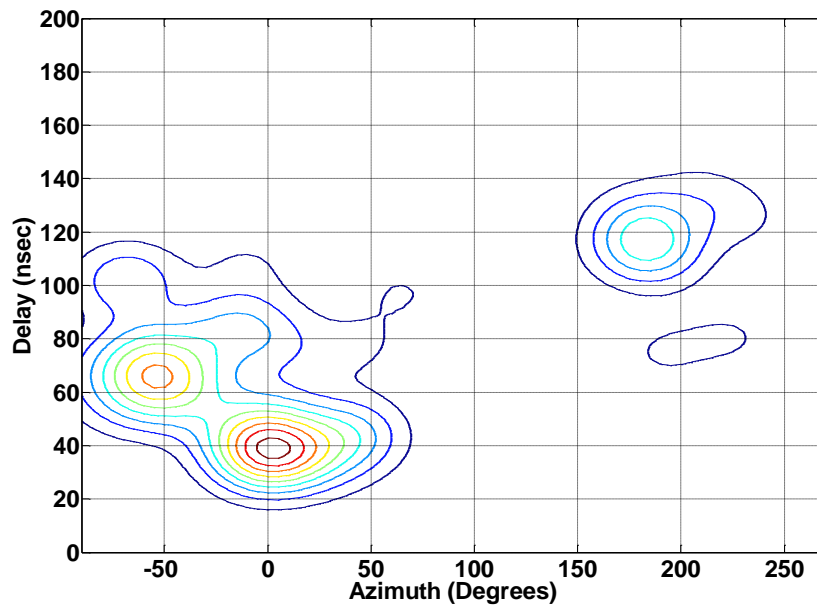


Fig (2-11): 2-D clusters in the office NLOS environment with TX omni antenna

time-angle space and the cluster's sizes are reduced. The RF energy transmission in that case is more focused toward certain direction and therefore, the impact of the scattering on the ray arrivals is reduced. Fig (2-12) displays the clusters at the receiver when a directional antenna with 30° 3-dB beamwidth is used at the transmitter. The directional antenna is facing the receiver in this experiment.

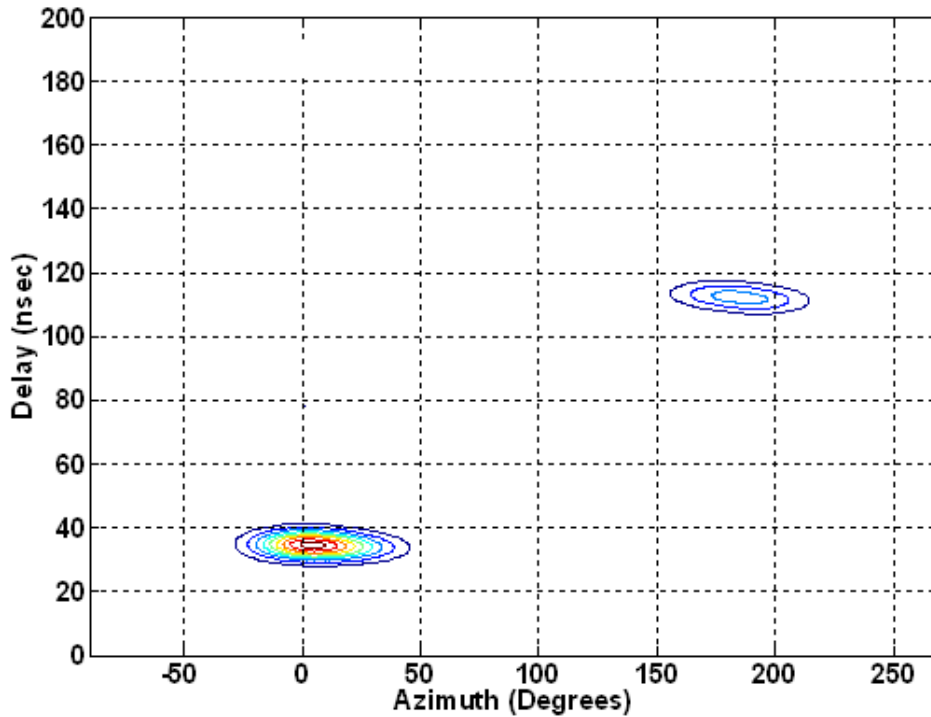


Fig (2-12): 2-D clusters $\alpha=30^\circ$ (Office NLOS environment, directional TX)

2.9 Conclusions

We have discussed the clustering characteristics of a millimeter wave indoor channel and the influence of geometry on this phenomenon. Knowledge of such spatial distribution of RF energy around the receiver in conjunction with array antennas and appropriate signal processing algorithms can lead to systems that provide superior performance by taking advantage of clusters' location and their corresponding characteristics. Also, statistical models that contain both angular and temporal components of the millimeter wave indoor channel are needed to ensure more efficient design of millimeter wave systems.

To simplify our analysis and simulations, we have assumed that most of the RF energy is confined in the horizontal plane. In other words, 3-D clustering (i.e. azimuth, elevation and time) has not been investigated. The complexity of making such 3-D measurements is an obstacle in achieving such information.

Chapter 3: Comparison of ray-tracing and millimeter wave channel sounding measurements

3.1 Ray-tracing

3.1.1 Motivation

Collecting a statistically significant database through measurements for each specific channel environment is an overwhelming task. Although in theory propagation characteristics of wireless channel could be accurately computed by solving Maxwell's equations with the building geometry as boundary conditions, clearly this approach is computationally intensive. Alternatively, this database can be generated by using simpler propagation models of the wireless channel, validated by measurement. Measurement, while essential to validate any other approach, is impractical in the scale necessary to cover a wide variety of wireless channel environments and system solutions. A prediction tool can be very valuable when designing a system for a specific environment or to predict wireless channel characteristics. In case of a valid tool, it can also serve, moreover, as a general performance evaluation tool, which can be employed to assess a large variety of wireless channel characteristics or parameter values. The tool saves on both time- and money- consuming installations; and in addition, it provides an environment for simulation and study of present and future wireless systems based on millimeter wave signals.

3.1.2 WiSE

In our investigation, we utilize the Wireless System Engineering (WiSE) package, which is a sophisticated ray-tracing tool developed and verified by Bell Laboratories [5], [18]. A symbolic ray-tracing of the WiSE is illustrated in the Fig (3-1). We exploit WiSE to compare the results of the deterministic ray-tracing simulation with empirical measurements obtained by the NICT in both home and office measurement scenarios (i.e. LOS and NLOS cases). In addition, we investigate the effectiveness of WiSE as a ray-tracing tool in creating wireless channel realizations for millimeter wave propagation in indoor environments. In the following, we briefly describe the way WiSE traces a radiated wave from a transmitter to receiver.

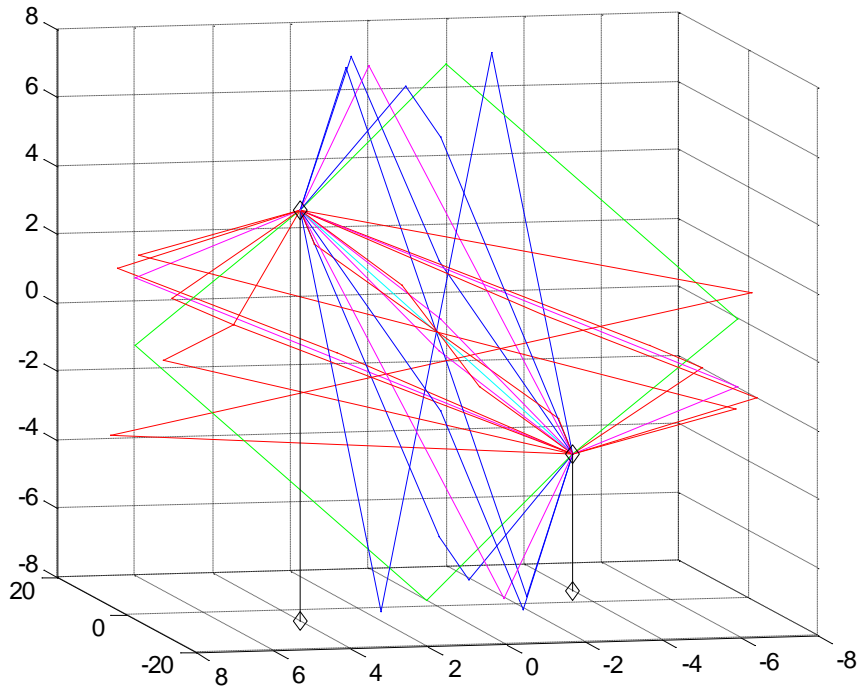


Fig (3-1): Sample output of WiSE

The principal challenge in predicting coverage is to cope with the potentially enormous combinatorial complexity of ray-tracing. Naively, each time a radio ray intersects a wall; it splits into a reflected ray and a transmitted ray, clearly an exponential process on the number of reflections. One simplification is to bind the maximum number of allowed reflections. A path from a transmitter to a receiver can then be specified by a sequence of reflecting objects. Through improved geometric prediction, the computation depends more on the number of useful rays than on the exponential number of possible rays.

WiSE provides the complex impulse response of the channel by accounting for all transmitted as well as reflected rays that arrive to the receiver location after an arbitrary number of reflections from environment objects. To calculate the arrival rays to the receiver location, the effects of the angle of incidence, the material dielectric constant and the transmitter and receiver antenna patterns are considered.

For each path, WiSE computes the loss according to the free space propagation loss, reflection and transmission coefficients and transmitter and receiver antenna radiation patterns. A sequence of computations starts with the direct path (i.e. LOS), followed by all paths with one-reflection, two-reflections, and so on. WiSE computes the reflection and also the transmission coefficients, for each physical object, from a multilayer dielectric model, maintaining angle and polarization dependencies. An arbitrary path is defined by the sequence of surfaces (walls, floor or ceiling) of which the signal must reflect to travel from the transmitting to the receiving antenna. Furthermore, it accommodates an arbitrary number of surfaces,

whether walls, floors or ceilings. WiSE stops calculating arrival rays to the receiver after a specified number of reflections or when the amplitude of a reflected arrival ray is lower than a threshold.

3.2 Comparison of ray-tracing results with measurement data

We have used WiSE to emulate the millimeter wave channel sounding experiment described in the previous section. The main difficulty in simulating an indoor RF channel is the strong dependence of the received signal on the layout of the building and all other obstacles inside (i.e. multipath channel). In particular, all walls, windows and other objects that affect the propagation of RF waves will directly impact the signal strength and more importantly the directions from which RF signals are received. Using ray-tracing will give us the opportunity to mimic the conditions of an indoor channel to the possible extent and at the same time provide a geometric interpretation of the results. The parameters of the simulation were set to closely match both the measurement environments and the process. The precise geometry of both the residential and the office environment were entered into the WiSE building modeler and in this way, the 3-D layouts of the measurement environments were constructed as seen in Fig (3-2) and Fig (3-3). Here, we have only focused on the room where the measurement was conducted and ignored the rest of the building layout. The assumption is that the signals that leave the room and bounce back inside are too weak to be considered. This is a valid assumption due to the usually high attenuation of the walls for millimeter wave signals.

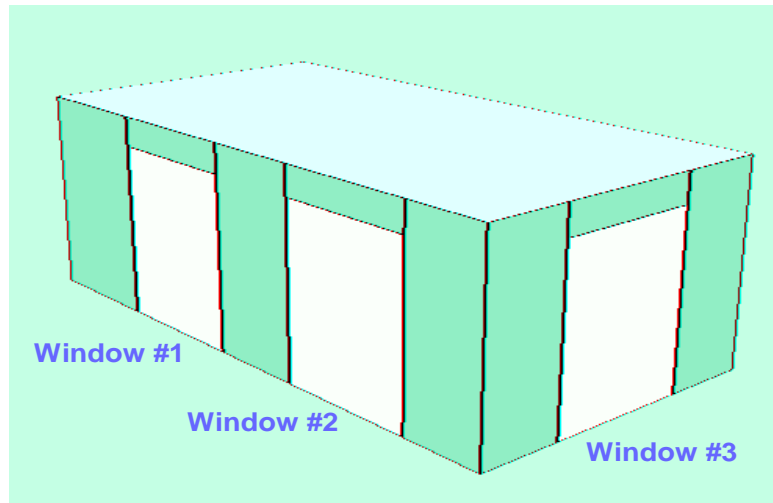


Fig (3-2): Ray-tracing residential layout

To reduce the complexity of the model representing the office environment, each row of tables with desktop computers (see Fig (2-4)) has been replaced by a wall-type obstacle of appropriate height and attenuation. This was done to re-create the NLOS condition between the receiver and transmitter. The radio characteristics of the walls (i.e. dielectric properties) were also chosen to approximately match the construction

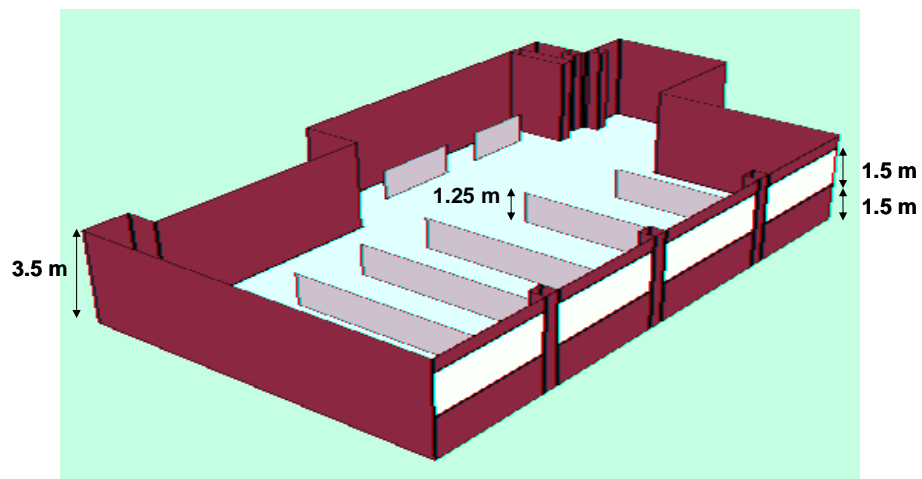


Fig (3-3): Ray-tracing office layout

materials of all objects in the measurement environments. 3-D Antenna pattern files were also created to match the gain pattern of all the antennas used in the experiment.

Finally, the measurement process was also re-created in WiSE by rotating the directional antenna at the receiver with 5° steps until full 360° coverage was obtained. For each direction of the receiver antenna, the frequency range of 61-64 GHz was swept by a continuous tone in steps of 7.5.MHz (3.75 MHz for the office) in order to generate the transfer function of the indoor channel. The complex two-dimensional impulse response of the channel was produced by using the same windowing function as in the VNA and then taking the inverse Fourier Transform of the data.

3.3 Space-time clusters and propagation environment correlation

In this section, the relation between the propagation environments and the space-time clusters is investigated. A comprehensive geometric interpretation of these results can be provided by considering the main paths that the RF signal travels between the transmitter and receiver as well as importing measured Power Delay Profile (PDP), and Power Angular Profile (PAP) into the layouts of the LOS and NLOS measurement setups (Fig (2-1) and Fig (2-2) in previous chapter). Fig (3-4) and Fig (3-5) illustrate the PDP of the arrival rays at the LOS direction and the PAP of the arrival rays at the time of the first LOS ray for the same measurement scenario.

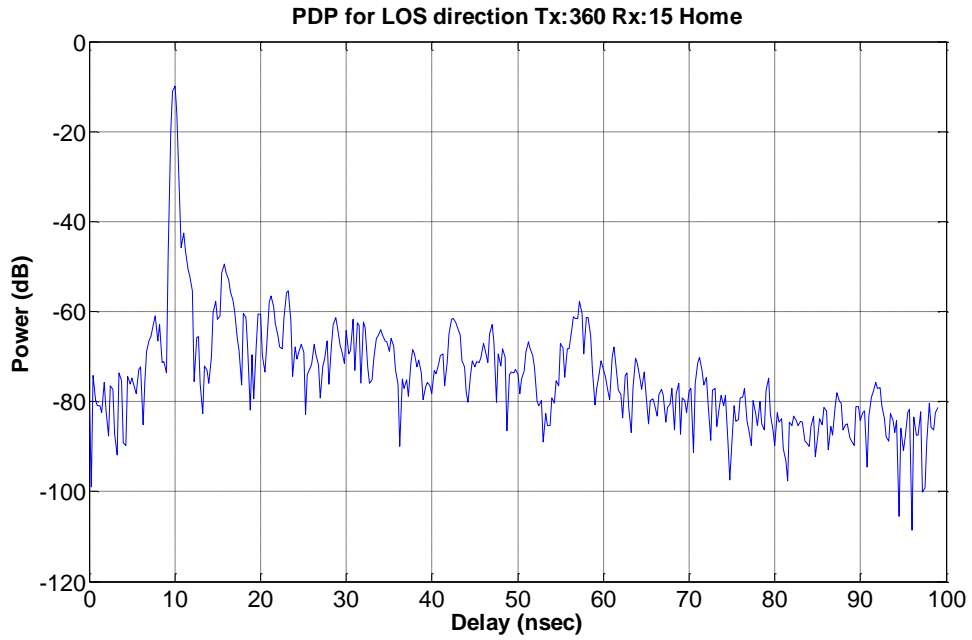


Fig (3-4): PDP of LOS arrival ray for TX: 360° and RX: 15° at LOS scenario

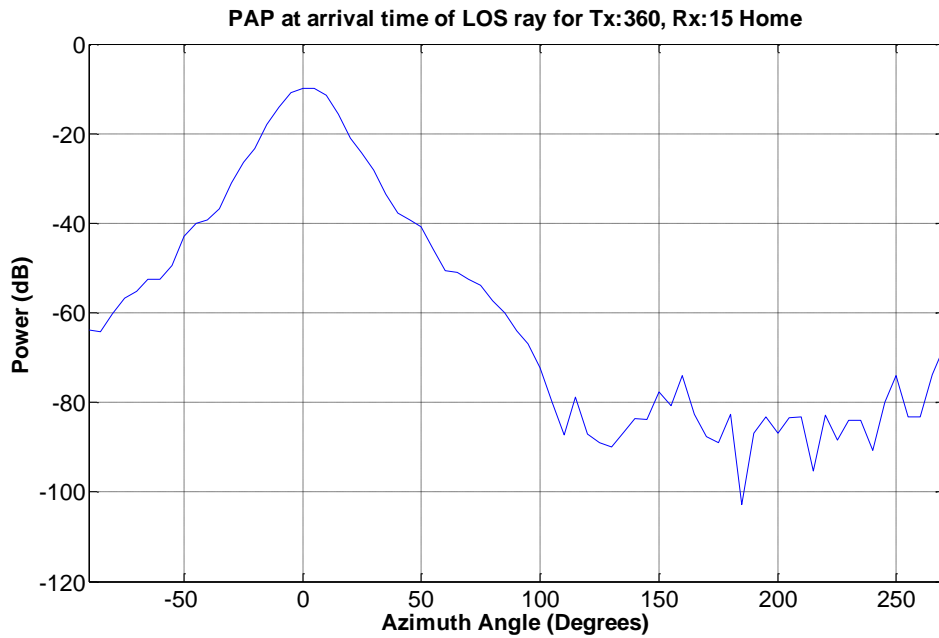


Fig (3-5): PAP at arrival time of LOS ray for TX: 360° and RX: 15° at LOS scenario

The one dimensional temporal clustering phenomenon has been observed in indoor channels and wideband statistical channel models have been proposed accordingly [8]. Here, we also observe that arrivals come in few groups (i.e. clusters) scattered in different coordinates throughout the time-angle space. These 2-D clusters are identified by using the KDE and an appropriate threshold representing the noise floor of the receiver. Fig (3-6) and Fig (3-7) display the clusters obtained by processing the measurement and simulation data when an omni-directional antenna is used in the residential environment. In general, strong resemblance in cluster shape and location is observed between the results derived from measurement and simulation.

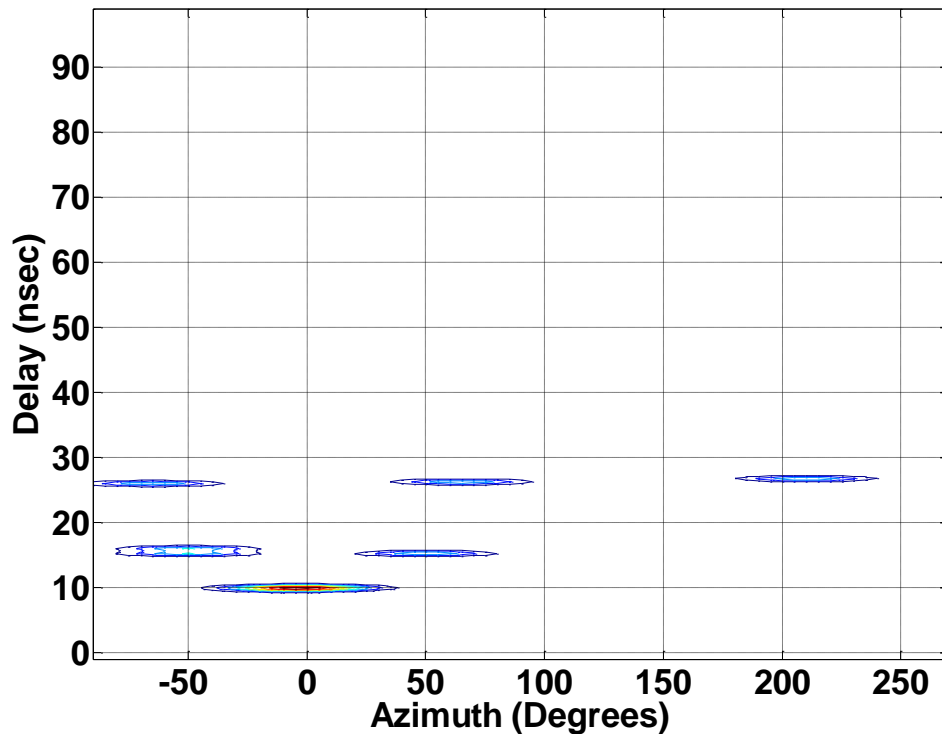


Fig (3-6): 2-D clusters identified from the measurement data in the residential LOS environment

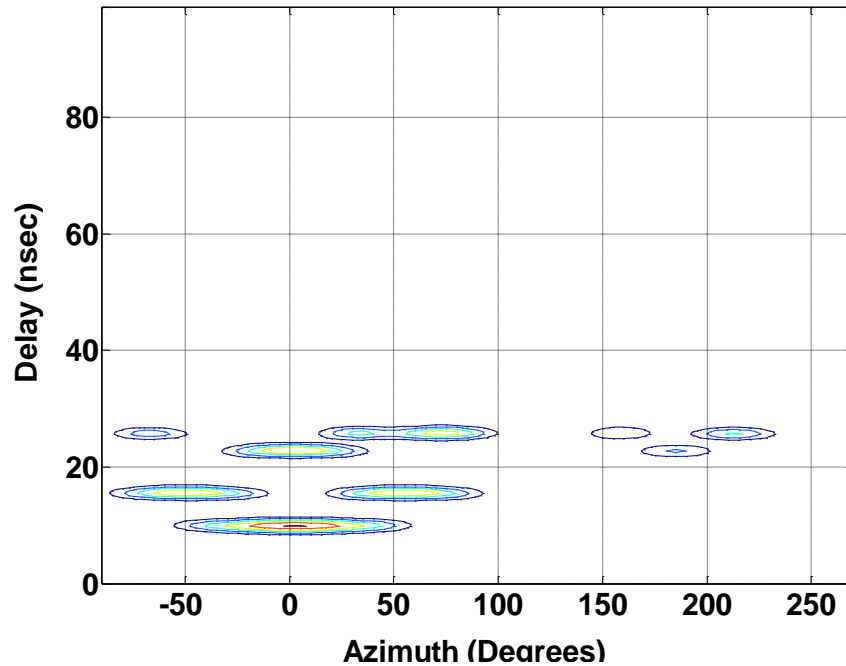


Fig (3-7): 2-D clusters identified from simulation data in the residential LOS environment

The ray-tracing simulation displays 9 clusters of arrivals at the receiver. The coordinates, of these clusters are listed in Table (3-1). Each cluster formation is the result of a unique path between the transmitter and receiver. These paths, which include direct LOS and various single-reflected and double reflected signals, have been graphically identified in Fig (3-8). Clusters 1 through 7 are also present in the measurement data with the exception that the clusters 6 and 7 have been merged and form a bigger cluster. Clusters number 8 and 9 which are the results of the reflection from the wall behind the receiver and transmitter respectively, are not present in the measurement data. This is due to the fact that the receiver and transmitter are positioned at the same height and the measurement equipment (e.g. covered by

electromagnetic absorbers in the case of the transmitter) blocks the path of the reflected signals from the back-wall. Such equipment does not physically exist in the

Table (3-1): Matched Cluster centers' coordinates

Cluster #	Cluster Arrival Angel (Degrees)	Cluster Arrival Time (nsec)	Exist in Experiment	Exist in Simulation
1	0°	10	Yes	Yes
2	-50°	15.5	Yes	Yes
3	50°	15.5	Yes	Yes
4	-74°	25.75	Yes	Yes
5	74°	25.75	Yes	Yes
6,7	152.5°, 207.5°	25.75	Yes (merged)	Yes
8	180°	22.75	No	Yes
9	0°	22.75	No	Yes

simulation; and therefore, these clusters form as a result of the reflection from both walls. We have also investigated the distribution of rays within a cluster in both measured and simulated data. Two types of distribution can be obtained: relative ray angle and time of arrival. The term relative indicates the angular or temporal displacement with respect to the cluster coordinates.

Fig (3-9) displays the distribution of the relative angle of arrivals for both measured and simulated data. Similarly, Fig (3-10) shows the distribution of the relative time of arrivals for both measured and simulated data. A close match for ray distribution is observed in both figures.

The data from the NLOS office environment was also processed for cluster identification. Fig (3-11) and Fig (3-12) demonstrate the achieved clusters for the measured and simulated data. The scattering effect of the furniture and other office

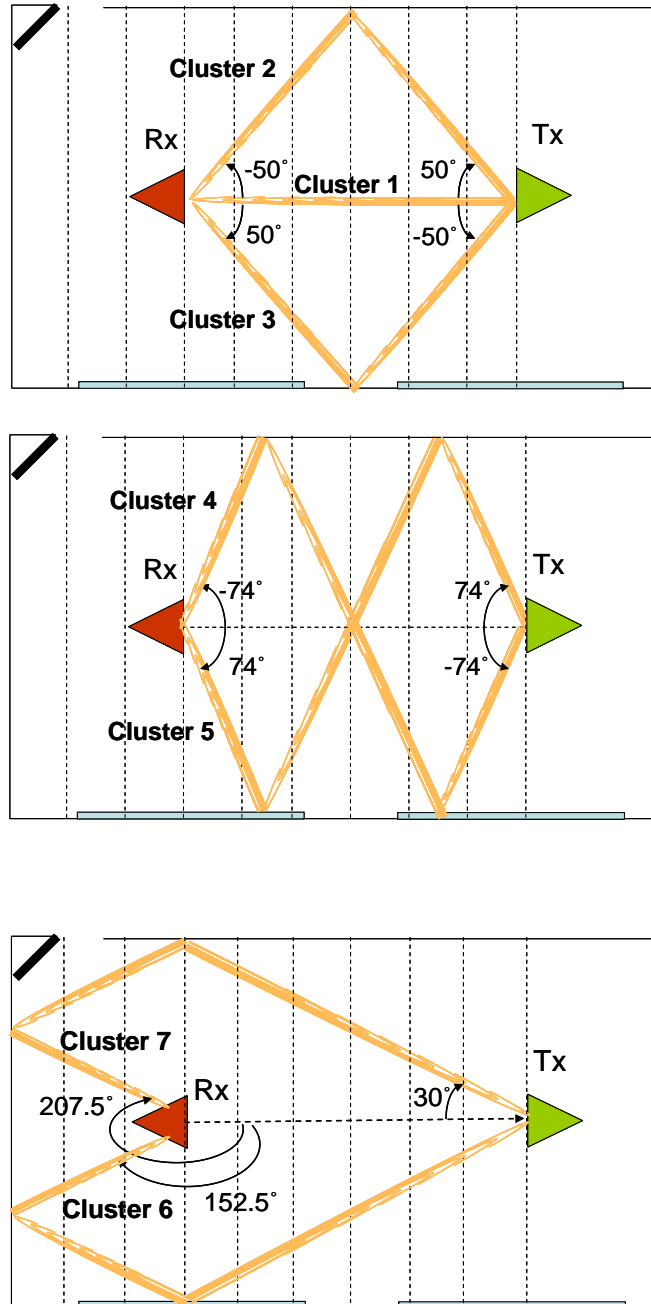


Fig (3-8): Cluster matching to the major arrival rays

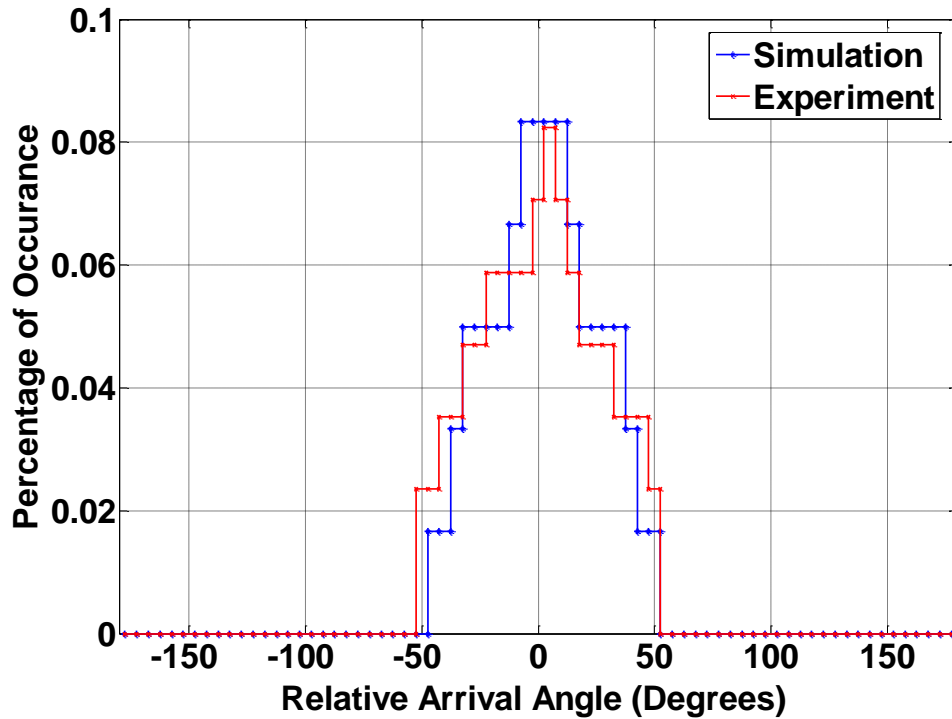


Fig (3-9): Distribution of the relative angle of arrivals

equipment in this environment, which cannot be accurately modeled by the ray-tracing tool, causes some differences in the shape and in some cases location of the clusters. Again, in general, 4 clusters are observed that are the results of the LOS and single-reflected paths. The clusters due to the reflection from the metal wall and the direct path between the transmitter and receiver have merged and form a bigger cluster in the measured data. As mentioned before, this is caused by the scattering effect that all the furniture in the office generates. The other two clusters occur because of the single reflection from the wall with glass windows and the wall behind the receiver. Looking at the time coordinates of the latter cluster, a mismatch is

observed between the results of the simulation and measurement. A physical explanation for this discrepancy can be given by noticing the velocity change of RF

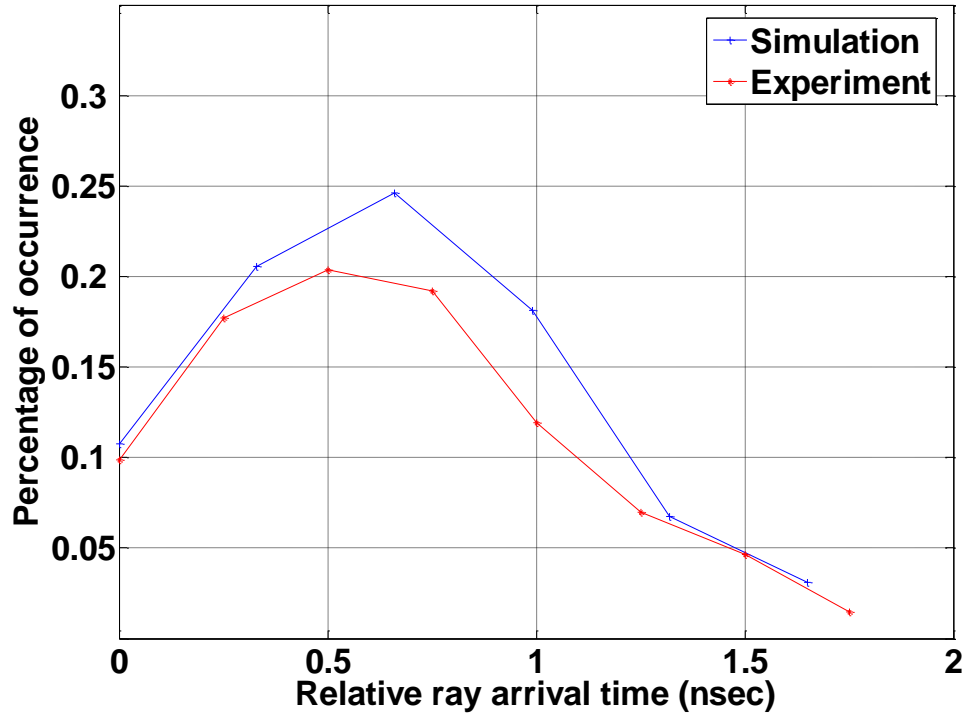


Fig (3-10): Distribution of the relative time of arrivals

waves as it goes through different materials that exist on its path between the transmitter and receiver [9]. In general, the exact coordinates, shape and size of the clusters depends on the details of the propagation environments. However, as seen in this study, the locations of the main clusters (i.e. high density) can be reasonably approximated by the ray-tracing tool.

The clusters in Fig (3-11) and Fig (3-12) are due to the use of an omni-directional antenna at the transmitter. If a directional antenna is used instead, the resemblance of cluster's shape and location obtained through measurement and simulation is

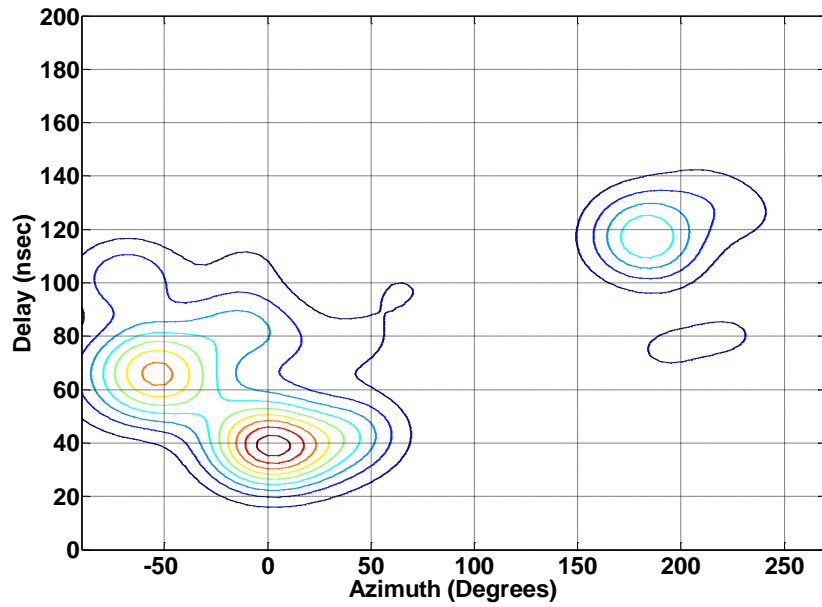


Fig (3-11): 2-D clusters identified from the experiment in the office NLOS environment with omni TX antenna

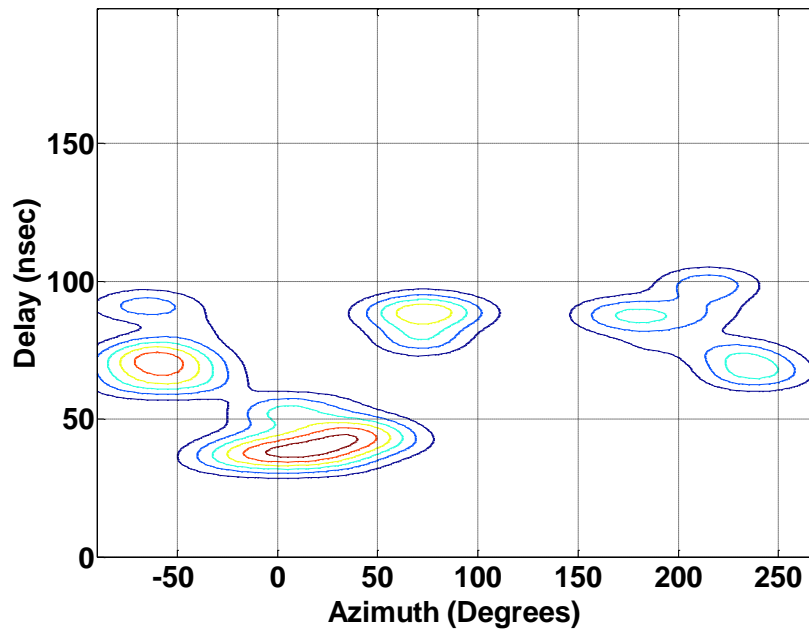


Fig (3-12): 2-D clusters identified from the simulation in the office NLOS environment with TX omni-antenna

increased. The RF energy transmission in that case is more focused toward certain direction and the impact of the scattering phenomenon on the ray arrivals is reduced.

3.4 Cluster energy

We have also investigated the energy distribution among the clusters in both residential and office environments. The normalized percentage of the received energy in each cluster is calculated as in [19], [22] and is referred to as the normalized relative energy.

Fig (3-13) and Fig (3-14) illustrate this percentage for omni and directional antennas in residential LOS and office NLOS environments respectively. It is seen that high percentage of the energy is concentrated in the first cluster. This is

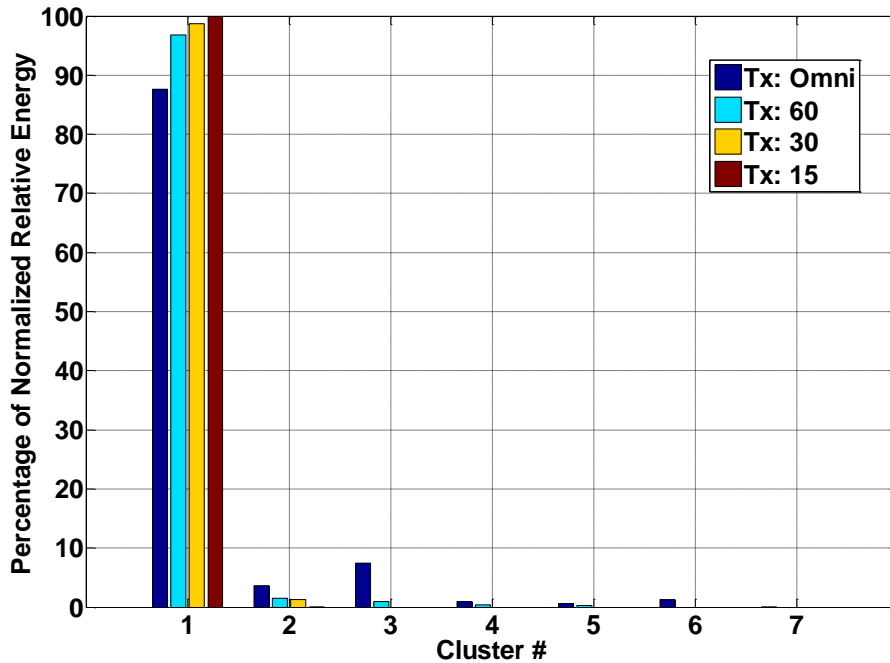


Fig (3-13): Percentage of Normalized cluster energy for different antennas in the residential LOS environment

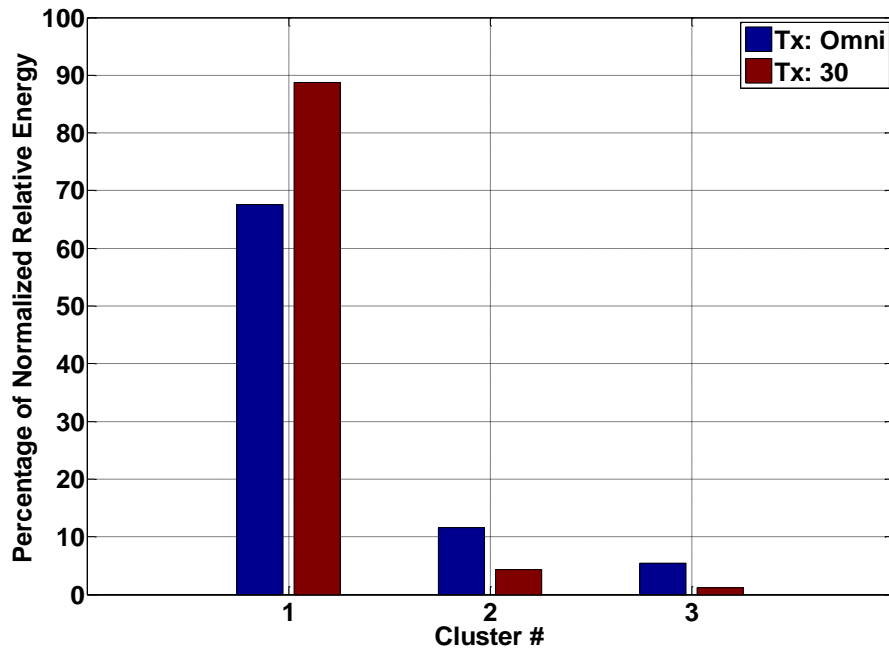


Fig (3-14): Percentage of Normalized cluster energy for different antennas
In the office NLOS environment

especially expected in the LOS case where reflected rays travel longer path and therefore contribute less energy to the corresponding cluster at the receiver. This might not be the case for NLOS cases in general. Also, as observed, using directional antennas with smaller beamwidths increases the energy of the 1st cluster. This means that for such scenarios, a single cluster statistical model is probably sufficient to describe the channel behavior.

3.5 Conclusions

In this chapter, we have captured the influence of geometry on the clustering phenomenon of a millimeter wave channel through the use of a ray tracing tool. We have shown that for indoor environments ray-tracing could be an effective tool to predict the location of the clusters around a receiver.

For scatter-free environments and LOS scenarios ray-tracing seems to provide a good match for cluster location and intra-cluster arrival statistics. For environments with heavy scattering, NLOS scenarios and directional antennas at the receiver and transmitter, ray-tracing prediction of the clusters still seems to be reasonably close to the results of empirical measurement.

Knowledge of the spatial distribution of RF energy around the receiver in conjunction with array antennas and appropriate signal processing algorithms can lead to systems that provide superior performance by taking advantage of clusters' location and their corresponding characteristics. According to the energy distribution among the clusters, a single cluster statistical model is probably sufficient to describe the channel behavior, while more experiments are required to verify and investigate this observation. Also, statistical models that contain both the angular and temporal components of the millimeter wave indoor channel are needed to ensure more efficient design of such systems.

Chapter 4: Optimal directional link establishment

4.1 Motivation

Millimeter wave technology is becoming increasingly important in many military and commercial applications. Remote sensing, radio astronomy, plasma diagnosis, passive imaging (e.g. imaging to display hidden contraband, weapons and nonmetal objects), radar and gigabit data rate communication are among these applications. To establish a high data rate communication link between two mobile nodes, acceptable Signal to Noise Ratio (SNR) at the receiver is required. However, due to the high propagation loss and signal attenuation that is associated with the millimeter wave signal, the communication range will be extremely limited.

Array antennas are an effective tool to manage the spatial transmission (or reception) of signals between two nodes. Using such array antennas, one would be able to increase the transmission range of millimeter wave systems [29]. An important property of array antennas for millimeter wave transceivers is their small physical size [28]. This property makes array antennas an attractive practical solution for establishing high range and reliable communication links between nodes in a network.

Utilizing appropriate signal processing techniques (such as beamforming), an antenna array will enable a transceiver to point its main lobe toward a desired direction. By focusing the radiation (or reception) pattern of an array antenna, higher communication range can be achieved. Alternatively, for a given communication range, lower power consumption can be expected. Also, chances of eavesdropping are

significantly reduced (low probability of intercept) since information is not broadcasted in all unnecessary directions.

The collection of all these benefits, points to using smart array antennas as a tool to control the spatial transmission and reception of signals between nodes. In this thesis, we are interested in using the beamforming capability to find the best possible directions for transmission and reception such that the communication link between two nodes provides maximal SNR at the receiver. To achieve this, an intelligent algorithm is required in order to choose the best (i.e. optimal) directions for the receiver-transmitter pair. For example, in urban or indoor environments where the radio line of sight is not necessarily the best propagation path between the two communicating nodes, this intelligent algorithm has to be able to simultaneously find the optimal directions for transmission and reception of the information. Similar techniques have been used for indoor mobile positioning and source direction estimation [25], [26]. Knowledge of the characteristics of the propagation channel can be exploited in order to select the best strategy for steering the beam pattern of the array antennas at the receiver and transmitter nodes [24].

4.2 Description and formulation of establishing an optimal directional link

Consider a system of two transceiver nodes A and B. We assume that each node is equipped with a circular array antenna that has beamforming capability. In other words, it is able to electronically steer its main lobe in the two-dimensional space (i.e. azimuth) toward any desired direction Fig (4-1). In addition, assume that each antenna is also capable of generating an omni-directional gain pattern as well.

The Received Signal Strength (RSS) is clearly a function of the directions where the main lobes of both antennas are pointing at. The directions that maximize the RSS are functions of both antenna patterns and the channel response (i.e. the environment). For environments with severe multipath propagation, it is important to locate these optimal directions in order to maximize the signal to noise ratio at the receiver. This is especially interesting in scenarios where the line of sight path has been blocked by an object with large attenuation.

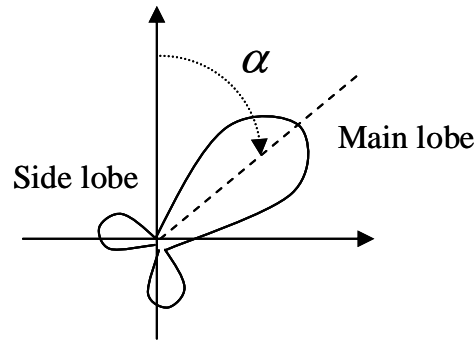


Fig (4-1): Beam steering in array antennas

Assume that $x(\theta, \alpha)$ denotes the transmitter's antenna gain at angle θ when the main lobe is pointing at direction α . Similarly, $y(\phi, \beta)$ denotes the receiver's antenna gain at angle ϕ when the main lobe is pointing at direction β . If $h(\theta, \phi)$ is the angular channel response for a path that starts from angle θ of the transmitter's antenna and ends at angle ϕ of the receiver's antenna, then the received signal R can be expressed as:

$$R(\alpha, \beta) = \iint_{\theta, \phi} x(\theta, \alpha) h(\theta, \phi) y(\phi, \beta) d\theta d\phi. \quad (4-1)$$

Here, for simplicity, we are also assuming that the propagation process is stationary. Our objective in this thesis is to find the optimal directions (α^*, β^*) that maximize the received power as defined below:

$$(\alpha^*, \beta^*) = \text{Arg max}_{\alpha, \beta} \|R(\alpha, \beta)\|^2 . \quad (4-2)$$

A simple method to find the solution of this problem is to conduct an exhaustive search over the space of all possible (α, β) . However, depending on the resolution of this space, this methodology might not be feasible for practical purposes. In this chapter, we propose a two step approach to find a sub-optimal value for the pair (α, β) . In the next sections, we will outline our approach and investigate its performance with simulation for different scenarios.

4.3 A protocol to establish an optimal directional link between two nodes

Step 1: Node A is in the transmit mode with an omni-directional gain pattern. This means that ideally, the transmitter's antenna gain for all azimuth angles is C where C is a constant. At the same time, node B is in the receive mode with beamforming capability. Initially, the main lobe of the receiver's antenna pattern is pointing toward a starting angle e.g. β_0 . Now, the beamformer rotates the main lobe around the 360 degrees field of view with a step size of Δ_B (i.e. $\beta_j = \beta_0 + j\Delta_B$). At each step, the receiver calculates the received signal strength and finds the direction

β_j where the RSS is maximal. If β_j^* denotes this angle, mathematically this step can be expressed by the following equations.

$$R(\beta_j) = 2\pi C \int_{\phi} \int_{\theta} x(\theta) h(\theta, \phi) y(\phi, \beta_j) d\theta d\phi, \quad (4-3)$$

$$\beta_j^* = \text{Arg max}_{\beta_j} \|R(\beta_j)\|^2. \quad (4-4)$$

Step 2: Now that the β_j^* have been obtained, node B goes into transmit mode and notifies node A that it has found its desired direction. Then, node A turns into a receiver with beamforming capability and the main lobe toward the starting angle α_0 . Next, the beamformer at node A rotates the main lobe around the 360 degrees field of view with a step size of Δ_A (i.e. $\alpha_i = \alpha_0 + i\Delta_A$). At each step, the receiver at node A calculates the received signal strength and finds the direction α_i where the RSS is maximal. If α_i^* denotes this angle, then mathematically this step can be expressed by the following equations.

$$R(\alpha_i) = \iint_{\theta, \phi} x(\theta, \alpha_i) h'(\theta, \phi) y(\phi, \beta_j^*) d\theta d\phi, \quad (4-5)$$

$$\alpha_i^* = \text{Arg max}_{\alpha_i} \|R(\alpha_i)\|^2. \quad (4-6)$$

If the beamwidths of the main lobes created by the array antennas at Nodes A and B are γ_A and γ_B respectively, then the rotation step size in the above protocol should obey the following equations

$$\Delta_A \leq \gamma_A,$$

$$\Delta_B \leq \gamma_B.$$

The beamwidths γ_A and γ_B depend on the size (i.e. number of elements) of the array antennas at nodes A and B. The choices for Δ_A and Δ_B clearly affect the speed with which the algorithm runs. Therefore, other hardware implementation issues might need to be taken into account.

In the next section, we provide simulations of this algorithm and show the effectiveness of the results.

4.4 Ray-tracing results

To investigate the effectiveness of the proposed algorithm, a simulation platform was implemented. The main difficulty in simulating a wireless channel is the strong dependence of the received signal on the surrounding environment (e.g. multipath channel). In particular, all obstacles such as walls, that affect the propagation of RF waves, will directly impact the signal strength and more importantly the directions from which RF signal energy is received. Empirical, statistical and deterministic models have been used to describe the behavior of such multipath channels [1], [30], [31]. In this study, we have elected to use a sophisticated ray-tracing tool to accurately predict the received signal strength in a multipath RF channel. The Wireless System Engineering (WiSE) software package is a ray-tracing tool that has been developed and verified by Bell Laboratories [5], [18]. We realize that even such models have limitations in their accuracy and are also subject to errors when there are

changes in the environment. However, this approach will give us the opportunity to simulate the performance of the proposed protocol in a multipath channel and at the same time provide a geometric interpretation of the results [36].

We first consider a very simple layout and two transceiver nodes (A and B) as shown in Fig (4-2). It is assumed that each node is equipped with a circular array antenna of a given size.

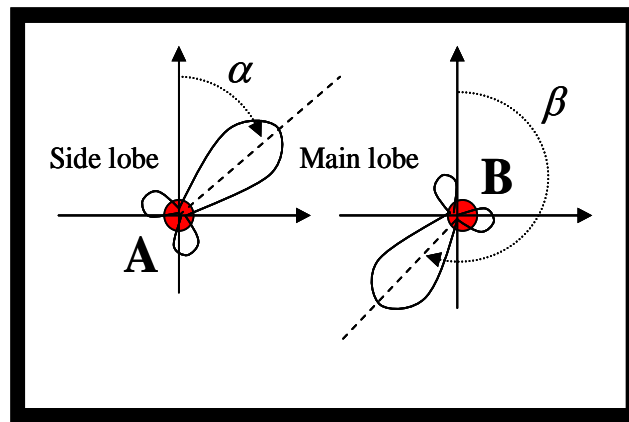
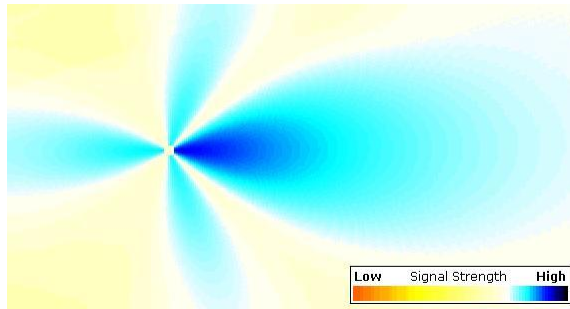
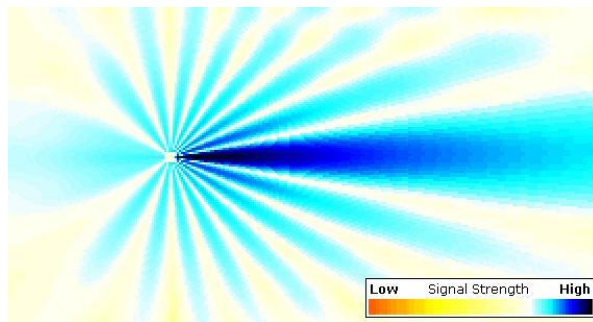


Fig (4-2): Ray-tracing layout

Having such an antenna with beamforming capability enables each node to steer the direction of its main beam towards any desired angle (i.e. 360-degree field of view). Sample beam patterns of such an antenna for various array sizes (i.e. number of elements) are shown in Fig (4-3).



(a)



(b)

Fig (4-3): Beam pattern of a circular array with: a) 8 elements; b) 32 elements

In general, the strength of the received signal depends heavily on the environment layout, dielectric properties of the surrounding material, transmitter-receiver locations, operating frequency and array sizes of the receiver and transmitter antenna. For the example given in Fig (4-2), the received power is a function of the azimuth angles of the main lobe of both the transmitter and the receiver. Fig (4-4) displays this received power as a result of simulation with a pair of 32 element circular array antennas at the receiver-transmitter pair and a transmission frequency of 60GHz.

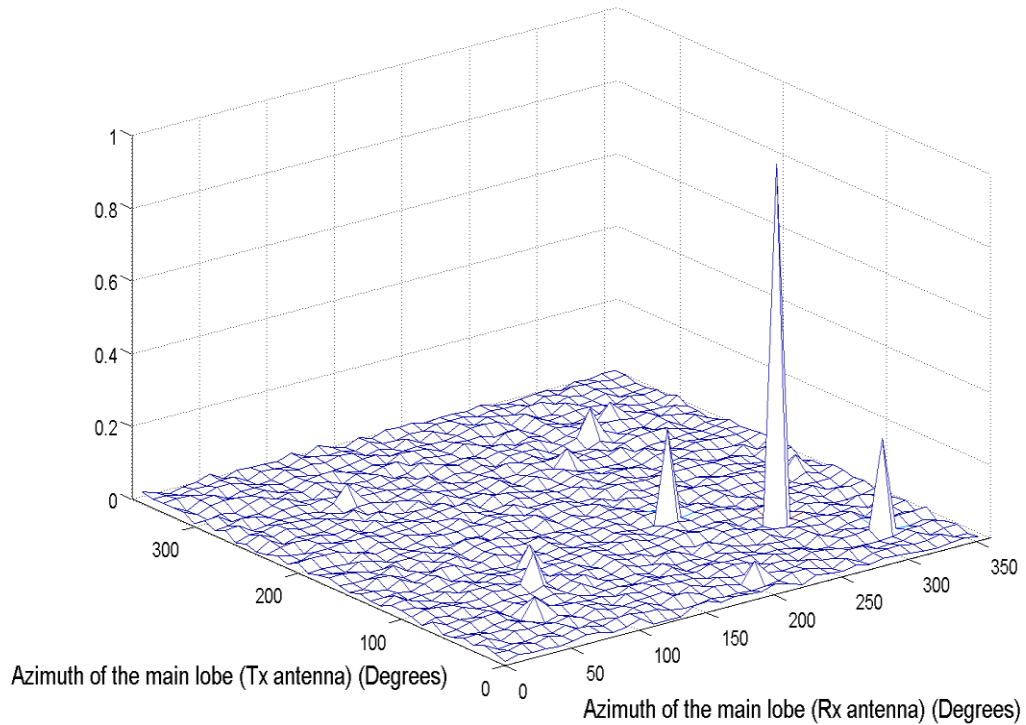


Fig (4-4): Normalized RSS as a function of the direction of the transmitter/receiver's main lobes

As observed, 12 different locations on this plot (i.e. pairs of (α, β)) exhibit received signal strength that are relatively stronger than other directions. These peaks correspond to the situations where the main lobes of the transmitter-receiver pair are positioned in a way to capture the line of sight, single-reflected and double-reflected signals respectively. Existence of a clear LOS path in this example signifies the strong RSS component that is visible at $\alpha = 90^\circ$ and $\beta = 270^\circ$. The link establishment

algorithm proposed in the previous section achieves these optimal directions (i.e. $\alpha = 90^\circ$ and $\beta = 270^\circ$) as symbolically shown in Fig (4-5).

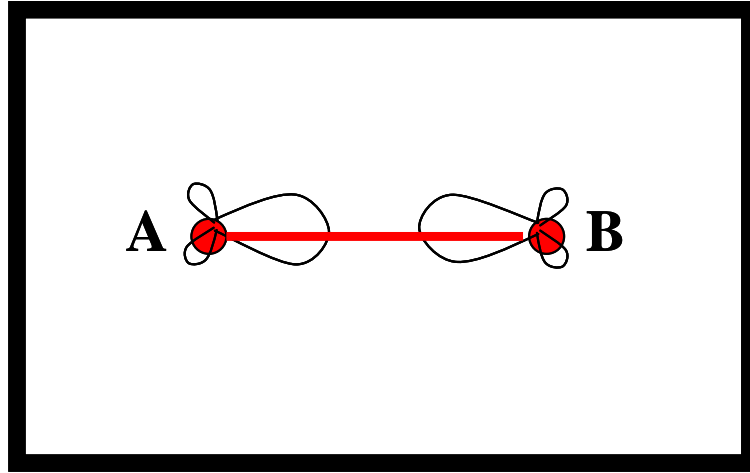


Fig (4-5): α, β selected by the link establishment algorithm

If this LOS path did not exist, for example due to an obstacle that blocks this path, then one of the propagation paths that contains a single-reflected signal will yield the best signal strength for the receiver. We also simulated this situation by ray tracing and Fig (4-6) shows the resulting link that our proposed algorithm has chosen.

This is indeed the optimal directions for the main lobes of the transmitter and receiver nodes as the simulation shows that the highest value of the RSS occurs at $\alpha = 40^\circ$ and $\beta = 320^\circ$ (see Fig (4-7)).

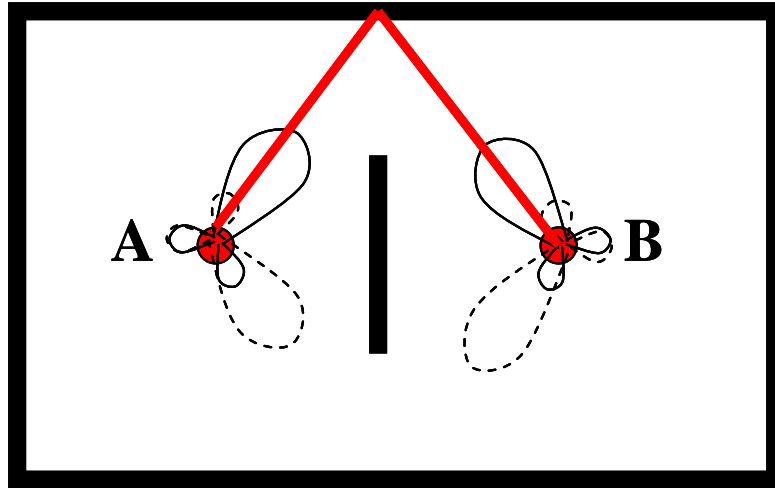


Fig (4-6): α, β selected by the link establishment algorithm.

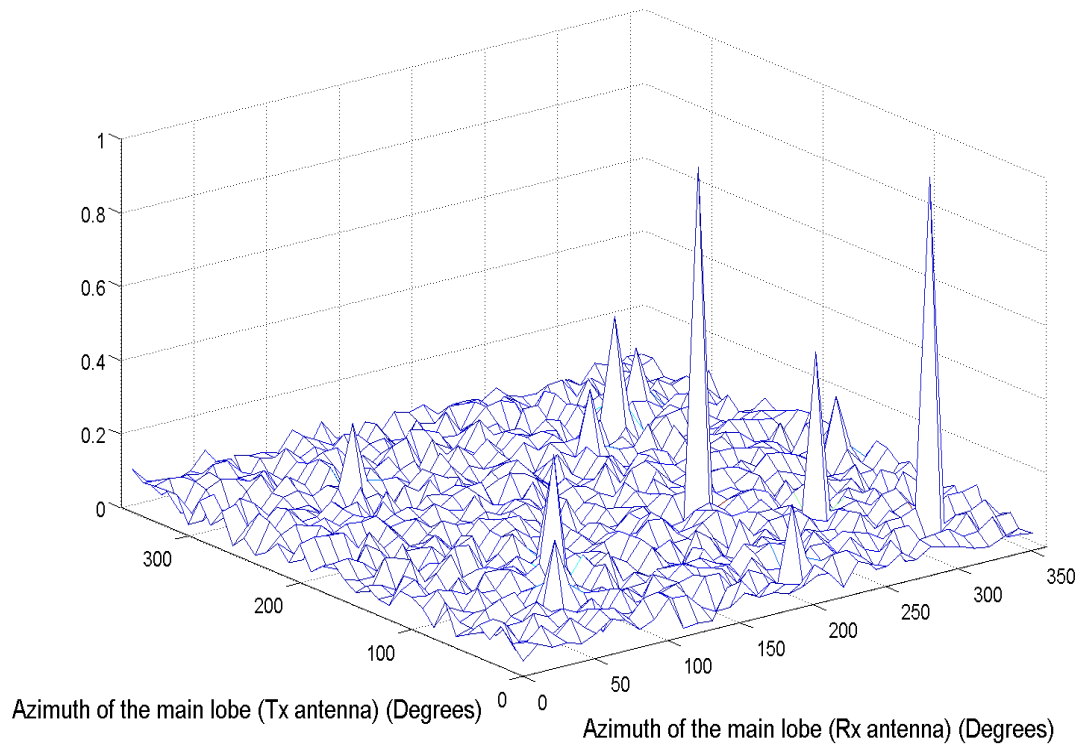


Fig (4-7): RSS as a function of the direction of the transmitter/receiver's main lobes

The direction pair displayed in this figure is also the optimal directions that could have been selected by exhaustive search of all possible directions.

The effectiveness of the link establishment algorithm was also investigated in a variety of other scenarios and some examples demonstrating the final direction, chosen for the main lobes of the antenna's beam pattern, are shown in Fig (4-8). These include single-reflected and double-reflected paths as they created the highest signal strength at the receiver.

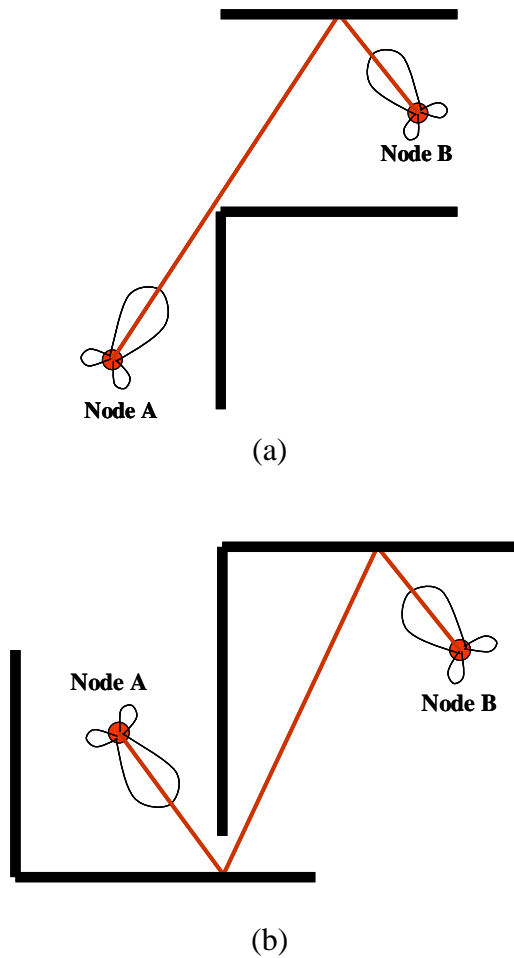


Fig (4-8): Optimal directions of the transmitter/receiver's main lobes: a) Single reflected path; b) Double reflected path

4.5 Conclusions

The underlying philosophy in this chapter is exploiting the information in the spatial distribution of RF energy around both transmitter and receiver results in better quality communication links. The proposed protocol outlines a methodology to obtain the directions, which the beam steering algorithms at the receiver and transmitter should use.

These directions achieve higher signal strength at the receiver; and therefore, a more reliable link can be expected. Although, all our simulations have shown that the selected directions are optimal, it is still conceivable that special scenarios could exist where the optimal directions are not achieved by the proposed algorithm. However, in order to capitalize on the capability of such antenna arrays, it is important to have an algorithm that can quickly converge to optimal (or near optimal) directions. The speed of this convergence is even more important when one or both of the communicating nodes are mobile. An adaptive version of the proposed algorithm will be an attractive solution for applications that involve mobile nodes.

Once the link is established, a power control mechanism can be implemented to reduce transmission power in order to conserve energy and prolong battery lifetime for mobile nodes. Minimizing the necessary transmission power also contributes to lowering the interference on spectrally co-existing systems. Therefore, multiple nodes can have simultaneous communication without affecting the reliability of each other's link. Finally, in many military and defense-related applications, where low probability of intercept is of paramount importance, avoiding wireless transmission in

all directions significantly reduces the chance for the RF signal to be detected by the enemy. This along with the fact that the large bandwidth available at millimeter wave frequencies results in very high data transmission rate, also helps to minimize the amount of time that a node needs to stay in transmission mode, and therefore, minimizes the possibility of its transmission being detected.

Chapter 5: Directional Medium Access Control (D-MAC), adapting the IEEE 802.15.3 MAC for millimeter wave technology

5.1 Introduction

Different networks may serve different geographic areas and subsequently have different implementations. The following networks have been defined based on coverage areas.

- a) Wide Area of Networks (WANs): A country or even the entire world
- b) Metropolitan Area Networks (MANs): A city or similar area
- c) Local Area Networks (LANs): A single building or campus
- d) Personal Area Networks (PANs): An area around a person

Recently, there has been huge interest in the last type of network, the PAN, for research and development. In a PAN, the group of connected devices is not referred to as a network, but rather as a piconet, to imply that it is small group of networked devices. In the PAN as shown in Fig (5-1), connected devices which are probably owned by a person should be able to have connectivity, data sharing and many new applications that are still developing.

One of the key characteristic of a PAN, that differentiae it from a LAN, is that a PAN usually consist of devices that are under the control of a single user. However, a LAN normally consists of devices that belong to multiple users. Another key feature of a PAN is peer-to-peer connectivity among the members of the PAN, although external connectivity is allowed.

To adapt the current IEEE 802.15.3 MAC layer of Wireless Personal Area Networks for Millimeter Wave technology, several considerations come into account. What features of millimeter wave technology do impact the current IEEE 802.15.3 MAC? How does the space-time clustering phenomena and geometric correlation of millimeter wave [37], [38] impact MAC design? What are the limitations



Fig (5-1): A Personal Area Network (PAN) with connected devices which might belong to a person

of the current IEEE 802.15.3 MAC layer for utilizing millimeter wave technology? In addition, how does the directional link establishment protocol, presented in [36], can be integrated into the designed MAC? In this chapter, the current IEEE 802.15.3 MAC layer is briefly reviewed; impacting features of millimeter technology on MAC layer design are discussed; limitations of the current IEEE 802.15.3 MAC layer are

described; and, finally the new D-MAC protocol designed to adapt the current IEEE 802.15.3 MAC layer of Wireless Personal Area Networks for Millimeter Wave technology is presented.

5.2 Overview of the current IEEE 502.15.3 MAC

In this section a brief overview of the current IEEE 802.15.3 MAC is given. A more comprehensive and detailed description of it can be found in [4].

5.2.1 Components of an 802.15.3 piconet

The piconet coordinator (PNC) and the device (DEV) are two key elements on the 802.15.3 piconet as shown in Fig (5-2). The size of the piconet is determined by

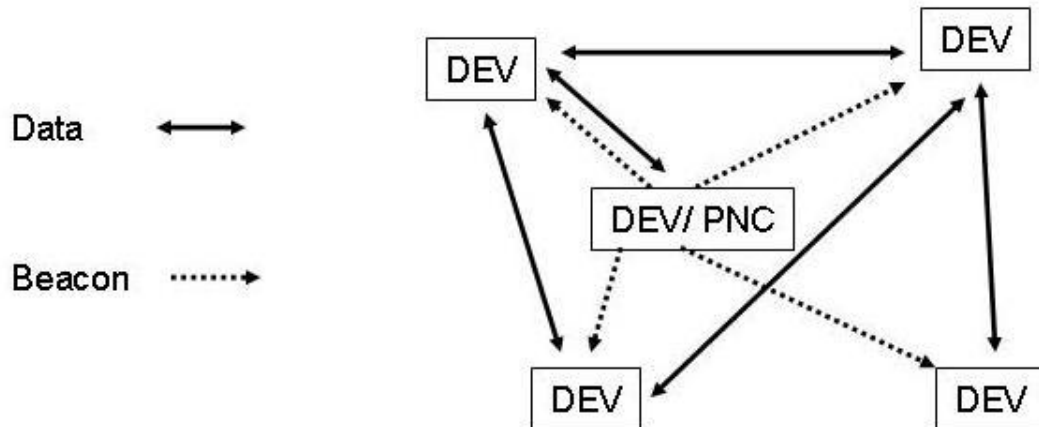


Fig (5-2): Elements of an 802.15.3 piconet

ability of the DEVs to hear the beacon transmitted by the PNC where the PNC is also able to communicate with any devices in the piconet. Without a PNC, it is not possible to form an 802.15.3 piconet. However, not all DEVs compatible with 802.15.3 are capable of becoming a PNC.

Therefore, the PNC is an essential element of every 802.15.3 network to operate suitably. The PNC has a variety of responsibilities as follows:

- a) Allocate channel resources among DEVS
- b) Provide the timing reference for the piconet via the beacon
- c) Provide approval of DEVs to join the piconet
- d) Manage the security and authentication process
- e) Keep track of sleeping DEVs to enable them to save power

5.2.2 Dependent piconet

A DEV in piconet can request channel time from the PNC to become the PNC of another piconet, called a dependent piconet. A DEV that is the PNC of a dependent piconet is referred to as a dependent PNC. The channel time of dependent piconet is shared with the original piconet, called the parent piconet. The dependent PNC is acting in two separate roles: one as a DEV in the parent piconet and another one as the PNC of another piconet that is timely synchronized to the parent piconet. An example is illustrated in Fig (5-3) where the dependent PNC is a member of both the parent and dependent piconet. This means one of the DEVs is a member of both the parent and the dependent piconet. This DEV needs to keep track of two personalities, one as a DEV in parent piconet and the second as a DEV in the dependent piconet.

5.2.3 Starting a piconet

At the first step of starting an 802.15.3 piconet, a PNC-capable DEV, begins to search channels to find other 802.15.3 piconets and to determine which channel has the least amount of interference. In case the DEV is unable to find another

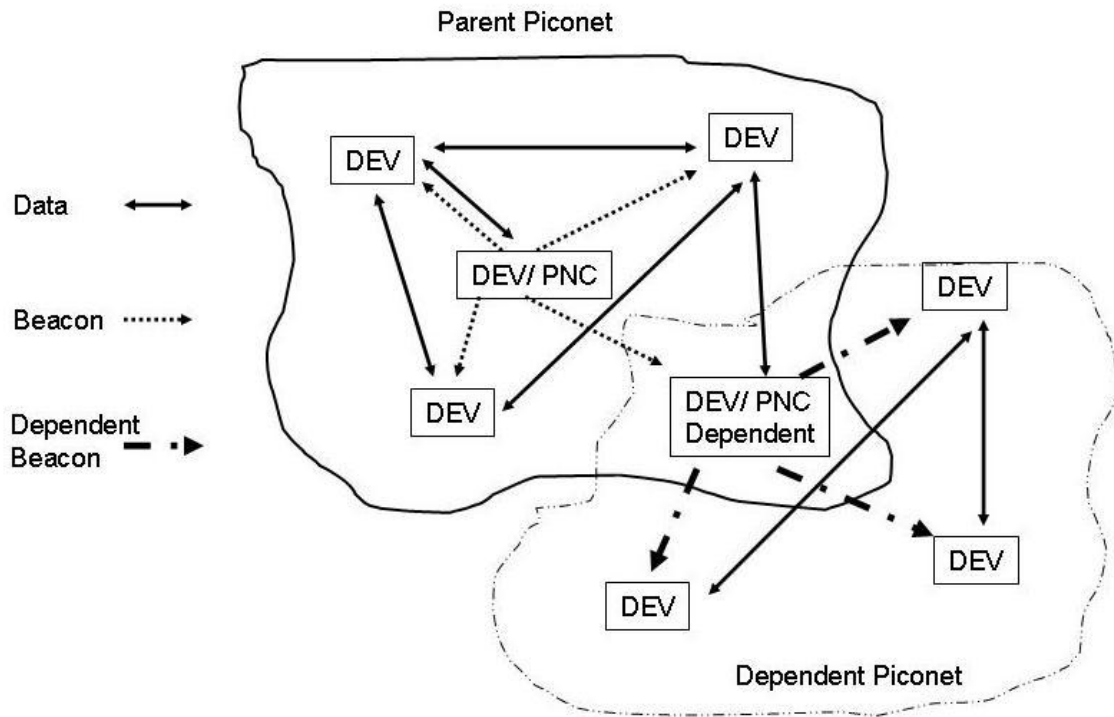


Fig (5-3): Parent and dependent piconet

802.15.3 piconet, it will start its own piconet by broadcasting a beacon. An 802.15.3 piconet is said to be in operation as long as the PNC is sending beacons, even when there are no other DEVs in the piconet. If for any reasons such as power outage, interference, etc., the beacon from PNC disappears, then after passing a time threshold, other DEVs in the old piconet have the option of starting a new piconet.

5.2.4 Structure of a superframe

The superframe is used by PNC to control timing and data transmissions among DEVs. A superframe as shown in Fig (5-4) consists of three parts:

- I. Beacon

- II. Contention Access Period (CAP)
- III. Channel Time Allocation Period (CTAP)

In the following, major role and functionalities of each part is described.

5.2.5 Beacons

Beacons are sent by the PNC to set the timing allocations and communicate management information. The beacon is sent by the PNC at a regular time instants such that the superframe duration is normally constant. The PNC can change the superframe duration size, but it announces the change to the DEVs in the piconet via the beacon before it makes the change. The beacon indicates the start and end times of the CAP and each Channel Time Allocation (CTA) as well as the start of the next beacon. Moreover, it includes information as which DEVs are sleeping and when they will be awoken.

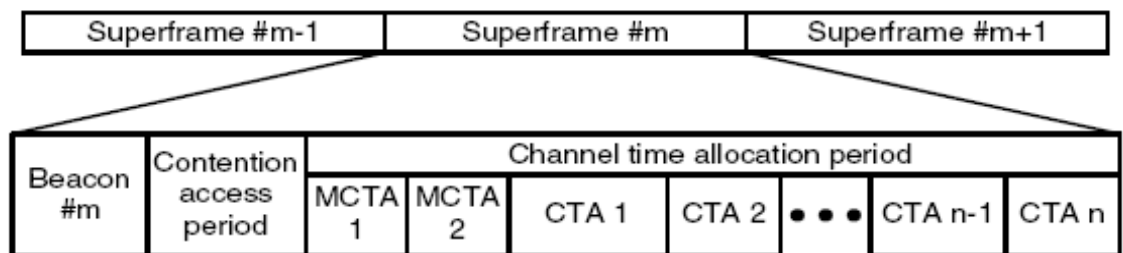


Fig (5-4): Superframe structure

5.2.6 Contention Access Period (CAP)

The CAP is used to provide efficient access for short bursts of data or command. The CAP is well suited for sending small amounts of asynchronous data between DEVs in the piconet because it doesn't require a formal channel time

reservation process. The CAP is also used by DEVs for association to the piconet. If the PNC feels that the CAP traffic in the piconet is low enough, it could skip allocating the CAP and the PNC may also set the CAP to be at zero length for some of the superframes. The CAP uses the access method of Carrier Sense Multiple Access Collision Avoidance (CSMA/CA) in a manner similar to 802.11, for exchanging commands and asynchronous data [11]. This access method allows an efficient use of the time for the CAP, while providing a low latency for DEVs that wish to send commands or data. When a DEV is going to transmit a frame in the CAP, it picks a random number from 0 to 7 to use as its backoff counter, n . It then waits until the channel has been clear for a specific period of time (i.e. $n \cdot P_{\text{Backoffslot}}$), and then gets to try and transmit its frame. The window size increases each time the frame is transmitted but it gets collided. The backoff window increases sequentially from (0 to 7) to (0 to 15), (0 to 31) and finally to (0 to 63). The DEV continues to use this backoff window until it gives up on sending the frame. Unlike 802.11, the counter is not reset if the medium is determined to be busy, and also the counter is not reset for each superframe. This means that regardless of whether the previous frame was sent successfully or not, the next frame uses backoff window of 0 to 7 for its first attempt to be transmitted during CAP. One reason could be that the CAP is only a small portion of total time in the superframe. If the DEV picked a long backoff counter with a short CAP, it might never get a chance to transmit a long frame.

5.2.7 Channel Time Allocation Period (CTAP)

The CTAP is composed of one or more CTAs that are allocated by the PNC to a pair of DEV identifiers. There are two types of CTAP: Management CTA (MCTA) and CTA. Only the DEV that is listed as source is allowed to transmit in a CTA and so the access method for CTAs is Time Division Multiple Access (TDMA) with guaranteed start and end times. In the case, PNC is the source or the destination of a CTA, it is called management CTA (MCTA). In most cases, there is no difference between an MCTA and a CTA. The only exception to this is when the source address is either the unassociated DEV or group of DEVs for broadcast. In this case, since there are multiple DEVs that are allowed to send information in the MCTA, where slotted ALOHA access method is used to handle potential collisions. The slotted ALOHA access method is very similar to the CSMA/CA mechanism in the CAP. Instead of using a backoff interval based on listening to the channel, the slotted ALOHA method uses the entire MCTA as a backoff slot and counts down until it can access the medium. However, unlike the CSMA/CA method, the DEVs using slotted ALOHA do not have to listen first to see if the medium is clear, they just transmit when they have counted down to their slot. Using MCTAs requires that the PNC keeps track of the potential needs of all DEVs in the piconet and assign MCTAs periodically to all of them. The DEVs need periodic MCTAs so that they can send commands to the PNC and maintain their association in the piconet.

5.3 Impact of millimeter wave technology on the current IEEE 802.15.3 MAC layer

Millimeter wave technology is a candidate PHY layer technology to be integrated into the current IEEE 802.15.3 standard. This could make feasible gigabit data rate communication among DEVs in a piconet. Achieving an acceptable Signal to Noise Ratio (SNR) at the receiver is required in order to establish a high data rate communication link between two mobile nodes. On the other hand, the communication range will be considerably limited due to the high propagation loss and signal attenuation that is associated with millimeter wave signals. The solution to overcome this inherent restriction of millimeter wave technology is exploiting directional antennas which is an effective tool to manage the spatial transmission (or reception) of signals between two nodes. One would be able to increase the transmission range of millimeter wave systems, using such directional antennas [29]. An important property of directional antennas for millimeter wave transceivers from an industrial point of view is its small physical size. This property makes directional antennas an attractive practical solution for establishing high range and reliable communication links between nodes in a network which is based on millimeter wave technology.

5.4 Limitations of the IEEE 802.15.3 MAC to exploit directional antennas

In many cases, to develop Medium Access Control (MAC) layer protocols for networking among individual nodes, the Physical (PHY) layer has been modeled by constructing simplified models. These models are unrealistic abstractions that make them easier to perform both analytical and simulation-oriented studies of the

developed protocols. For example, considering omni-directional antennas, in the model of Unit Disk Graph (UDG), communication behaviors are categorized in three ranges based on distance from antenna. As shown in Fig (5-5), the first area which is the closest one to the antenna is the transmission range on which communication is possible with low error rate. The next one is the detection range at which detection of signals is possible, but no communication is possible. Then, the far-out area is the interference range at which signals may not be detected, and they are added to the background noise.

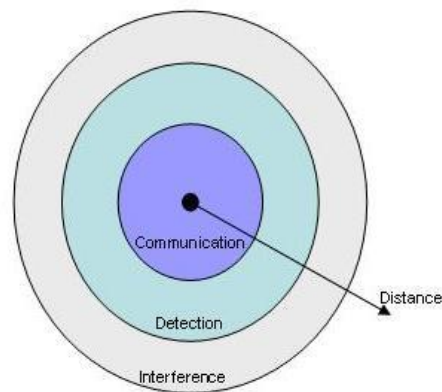


Fig (5-5): Unit Disk Graph model (UDG)

Based on the previous section, directional antennas are needed for establishing high range and reliable communication links between nodes in a network which is based in millimeter wave technology. The current IEEE 802.15.3 MAC layer had been developed by considering omni-directional antennas for both transmitter and receiver of DEVs and PNC. This means the medium is shared among all nodes based on a PHY layer model similar to the one described above where all directions around the antenna are equally treated from the communication point of view. Moreover, neighbor discovery by DEVs, starting a piconet, beacon broadcasting by PNC,

contention among DEVs and or data transfer between DEVs or between PNC and DEVs are communicated using omni-directional antennas. Therefore, the current IEEE 802.15.3 MAC layer should be adapted for millimeter wave technology which exploits directional antennas. In the next section, a solution is presented to adapt the current IEEE 802.15.3 MAC layer of Wireless Personal Area Networks (WPAN) for millimeter wave technology.

5.5 Directional Medium Access Control (D-MAC)

The current IEEE 802.15.3 MAC layer needs to be adapted in order to work effectively with millimeter wave technology which exploits directional antennas. There are several challenges that should be addressed. Neighbor discovery where transmitter and receiver antennas are both omni-directional is trivial. However, directional neighbor discovery in the case where each one or both of the transmitter or receiver antennas are directional is challenging. PNC to DEV or DEV to DEV communication is another challenge. The structure of the superframe should be modified in a way that it can support directional antennas. The modified MAC should have backward compatibility. This means interoperability with DEVs that only employ omni-directional antennas should be still feasible. A solution for adapting the IEEE MAC to support directional antennas is provided which addresses these challenges. In this solution, two directional superframes are introduced. A Long Directional superframe (LD-superframe) is defined to address directional neighbor discovery, and a Short Directional superframe (SD-superframe) is introduced for regular piconet activities. In the following, first basic operations of a piconet of DEVs

with directional antennas are expressed. Second, directional neighbor discovery is described, and finally directional link establishment is presented.

5.5.1 Basic D-MAC operations of a piconet of devices with directional antennas

As shown in Fig (5-6), the basic operations of a piconet which includes DEVs with directional antennas can be categorized as follows.

i. Starting a piconet

A DEV searches an active operational piconet using passive scanning for a period of time. In case, no desired or connectable piconet is found, the DEV starts a piconet. Otherwise, the DEV tries association to the found piconet.

ii. Directional neighbor discovery

After a PNC initiates a piconet, directional neighbor discovery procedure starts. This procedure is occasionally performed to allow DEVs with omni-directional or directional antennas to join the piconet. The PNC transmits long omni beacons.

iii. Association

The DEV receives a beacon frame, the association process for DEVs starts.

iv. Beacon broadcasting

The PNC transmits omni beacon. DEVs detect the beacon frames by scanning in all directions.

v. Directional Link Establishment (DLE)

A DEV that wants to communicate with another DEV using a directional antenna, asks the PNC for required time to establish directional link.

vi. Data transmission

After establishing directional link, the DEV requests desired channel time from PNC to send data stream. In case, resource is available, the PNC allocates the reserved time for the data stream, and directional communication starts.

vii. Disassociation

If a DEV or PNC wants to drop out from a piconet, the disassociation process starts.

viii. Stopping piconet

After the PNC drops out, the piconet is stopped.

5.5.2 Directional neighbor discovery

If transmitter and receiver both have omni-antennas, then neighbor discovery is trivial. However, if each one or both of the transmitter or receiver antennas are directional, then a directional neighbor discovery procedure which utilizes actual antenna beam patterns is challenging. The transmission pattern of a directional antenna is complex and difficult to model. Most of the proposals for directional neighbor discovery so far are based on simplified (unrealistic) antenna beam patterns. In [32], [33], [34] nodes have omni-directional antennas but, they must be equipped with Global Positioning System (GPS) for functionality of the algorithm. In the Direct Discovery algorithm of [35], nodes discover their neighbors only upon receiving a transmission from their neighbors but, the AoA or location information of the neighbors is essential for further communication after the discovery phase, where receiving a signal from neighbors while both nodes have directional antennas has been addressed. On the other hand, in the Gossip-based algorithm [35], nodes gossip

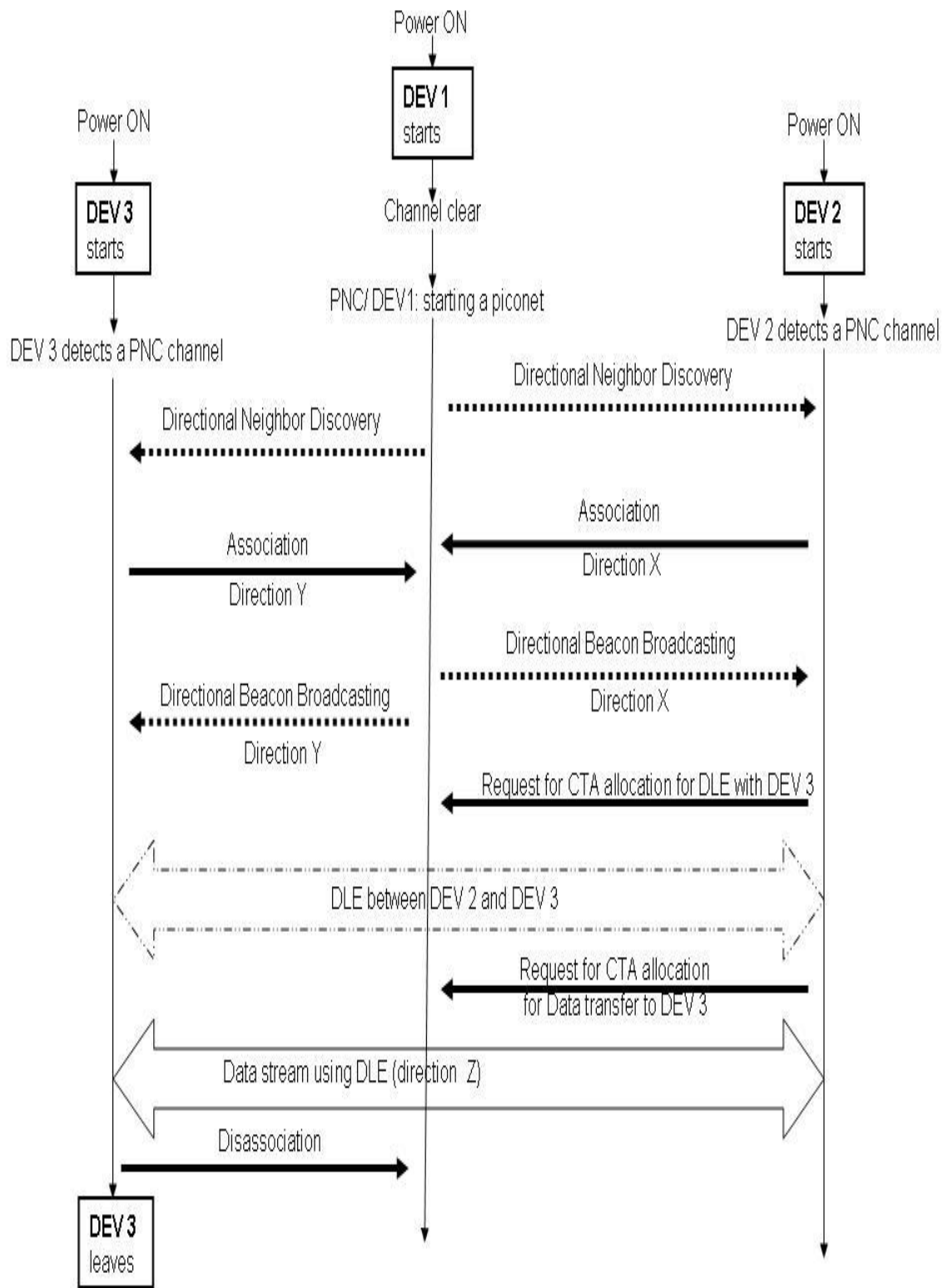


Fig (5-6) Basic operation of piconet of DEVs equipped with directional antennas

about their neighbors' location information to enable faster discovery, but all nodes should be equipped with a GPS receiver to know their location information.

A Long Directional superframe (LD-superframe) is defined and utilized by the PNC to detect DEVs with omni or directional antennas without any prior arrangement or sharing location information between them. Moreover, the DEVs are not required to be equipped with GPS and or location information of the DEVs. The LD-superframe is run by PNC whenever it wants to detect neighbor DEVs. The rate of utilizing LD-superframe by the PNC depends on available resources at the PNC such as free time slots and power. In other words, whenever the piconet is larger and it has more devices and consequently lower free time slots, the PNC checks for interested DEVs less. On the other hand, if there are a few DEVs in the piconet and many free time slots, the PNC runs LD-superframe and checks for possible DEVs to join very often. Another policy is to run LD-superframe on a regular basis which has a simpler implementation. The structure of the LD-superframe is shown in Fig (5-7).

Long Directional Beacon Period (LD-BP)	Long Directional Contention Access Period (LD-CAP)						Channel Time Allocation Period (CTAP)								
Long Omni Beacon (LOB)	G B	LD-CAP Omni	G B	LD-CAP Direction 1	G B	LD-CAP Direction m	G B	MCTA	G B	CTA 1	G B	CTA n	G B

Fig (5-7): Long Directional superframe (LD-superframe)

In the Long Omni Beacon period (LOM), the PNC broadcasts a long omni beacon. Transmitting beacon in omni direction is similar to the current IEEE 802.15.3

MAC. This omni directional beacon broadcasting provides backward compatibility for devices which are not equipped with a directional antenna. The LOB is long enough that a potential DEV that is in receiver mode and looking to join the piconet can scan all directions. This scanning is similar to *step 1* of the directional link establishment (DLE) protocol described in section 4.3. At the end of the LOB, a potential DEV has figured out β_j^* , the direction it should use to get the maximum of RSS from the PNC.

In the Long Directional Contention Access Period (LD-CAP), the PNC dedicates a regular omni CAP for DEVs with omni communication capability followed by directional CAPs for all directions. These CAPs are separated with appropriate guard bands. The omni CAP is provided to support backward compatibility for devices without directional antennas. Since at this stage, the PNC is not still aware of the receiving direction that a potential DEV may try to associate to the piconet for the first time, the PNC has to scan CAPs in all directions for transmitted signals from potential DEVs. This scanning is similar to *step 2* of the directional link establishment protocol described in section 4.3. At the end of LD-CAP, the direction of α_j^* is known for the PNC, which is the direction that the PNC should use to get maximum RSS from the DEV. This means that the PNC and the DEV have followed the protocol described in section 4.3; they have established a directional link and they are aware of the optimal directions for communicating with each other from now on.

Finally, the last part of an LD-superframe is the Channel Time Allocation Periods (CTAP), which are assigned by the PNC for communication of the PNC to

the DEVs or DEV to DEV. The CTAP in a LD-superframe are similar to the CTAP in the superframe of the current IEEE 802.15.3 MAC.

This directional neighbor discovery does not need any prior arrangement or shared location information between PNC and DEV. There is no time synchronization between PNC and DEV. More over, none of PNC or DEV is required to be equipped with GPS. Different transmitter or receiver antennas could be used at DEV while the DEV can still be detected. The directional neighbor discovery is based on the algorithm described in the previous chapter where PNC and DEV discover each other and, they are able to establish an optimal directional link by following *step 1* and *step 2* of the algorithm. The neighbor discovery is based on actual antenna patterns of the nodes, and the established link does not require direct sight of view between two nodes (i.e. LOS) as shown in Fig (4-6), and Fig (4-8).

5.5.3 Integration of directional link establishment

When the PNC is not in the directional neighbor discovery mode, it doesn't need to use LD-superframe. Instead, it uses SD-superframe where directional beacons are broadcast and directional CAPs are allocated only to directions of the optimal directional links established between PNC and DEVs. A SD-superframe includes Short Directional Beacon Period (SD-BP), Short Directional Contention Access Period (SD-CAP), and CTAP.

As illustrated in Fig (5-8) in the SD-BP, beacons are broadcast in omni and only to directions of communication that were established during the neighbor discovery phase. This means, in SD-superframe, the PNC does not dedicate directional CAPs for all directions; it rather allocates omni and directional CAPs only to directions that

already associated DEVs to the piconet are communicating. In addition, appropriate guard bands are separating omni or directional beacons and also CAPs from each other. Omni beacon and omni CAP are provided to support backward compatibility for devices which are not equipped with directional antennas.

Short Directional Beacon Period (SD-BP)						Short Directional CAP (SD-CAP)						Channel Time Allocation Period (CTAP)								
SDB Omni	G B	SDB Dir i	G B	SDB Dir j	G B	SD- CAP Omni	G B	SD- CAP Dir i	G B	SD- CAP Dir j	G B	MCTA	G B	CTA i	G B	CTA j	G B

Fig (5-8): Short Directional superframe (SD-superframe)

Whenever two DEVs want to communicate using directional antennas, they first need to establish a directional link prior to starting data stream transmission. For this purpose, the DEV which wants to initiate communication with another DEV asks for allocating required CTA from the PNC. Then, during the allocated CTA, it follows the directional link establishment protocol similar to the one which has been described in chapter 4. After establishing the directional link, both transmitter DEV and receiver DEV are aware of the best direction that they can communicate. After establishing the optimal directional link, the transmitter DEV requests from the PNC to allocate CTA for data stream transfer. Transferring data stream takes place in the allocated CTA between two DEVs through the established directional link.

There has been a tendency in the standard to keep most of the complexity, whenever possible, in the DEV. This allows the DEVs to be as complex as they need

to be to support their applications without burdening the DEV that happens to be the PNC. The same policy has been followed for channel time allocation for directional link establishment or data stream communication through the established link. Instead of sending the required beamforming sectors, data rates, buffer size, latencies, and priorities to the PNC so that it can determine the appropriate amount of channel time, the DEVs are simply required to calculate the amount of channel time that they need for their application and the frequency with which it needs to be allocated. On the PNC side, the PNC simply decides whether there is enough resource to allocate the channel time, and in that case the PNC allocates the requested time slots. On the other hand, since not all the DEVs are required to be PNC capable, this allows very low cost devices such as wireless speakers.

5.5 Conclusions

In this Chapter, a new D-MAC protocol compatible to the current IEEE 802.15.3 MAC in order to support millimeter wave technology exploiting directional antennas is given. The new designed structure and basic operations of the D-MAC are described. LD-superframe and SD-superframe are introduced. The D-MAC has backward compatibility with the IEEE 802.15.3 MAC, and it can still support devices which are not equipped with directional antennas. More over, a directional neighbor discovery algorithm based on the directional link establishment algorithm is presented which does not require time synchronization or any location information of the communicating nodes. The neighbor discovery provides the capability that two nodes equipped with directional antennas can discover and communicate based on their actual antenna patterns and also independently of the existence of LOS between them.

Chapter 6: Summary of contributions and directions of future research

6.1 Summary of contributions

By analyzing measurement data of millimeter wave channels for the indoor environment, space-time clusters are identified. Intercluster statistics for millimeter wave propagation are calculated. Correlation of the identified space-time clusters to the propagation environment is determined.

The effectiveness of the ray-tracing method in creating channel realizations in the intercluster and intracluster levels for millimeter wave indoor environments is validated.

A protocol to establish an optimal directional link between two nodes equipped with directional antennas is presented. The correctness of the protocol for different scenarios is evaluated and illustrated using a ray-tracing tool.

A new Directional Medium Access Control (D-MAC), which is compatible with the current IEEE 802.15 MAC of WPAN for millimeter wave technology exploiting directional antennas, is designed. The new D-MAC can still support devices that are not equipped with directional antennas.

Finally, a new directional neighbor discovery algorithm is presented, which does not require time synchronization or any location information of the communicating nodes. This means that two nodes equipped with directional antennas can discover and communicate with each other using the presented D-MAC.

6.2 Future research

Millimeter wave technology is still in its early stage of development. Space-time behavior of millimeter wave channels for LOS and NLOS indoor environments have been presented. Additional measurement for a variety of indoor and outdoor environments is required to extract a comprehensive statistical millimeter wave channel model. Especially experimental data based on directional antennas with narrow beamwidths (e.g. less than 5 degrees) at the transmitter and the receiver provides opportunity to accurately calculate intracluster statistics and also to investigate arrival ray behaviors. Correlation of arrival rays in the time and angle domains can be analyzed and its possible relation to geometry of propagation environment can be studied. Moreover, millimeter wave behaviors for Multiple Inputs Multiple Outputs (MIMO) channels can be investigated. A ray-tracing tool can be used as a cost-effective and fast tool to predict the channel behavior.

The directional link establishment protocol introduced in this thesis provides an optimal link between two nodes equipped with directional antennas. The established directional link achieves higher signal strength at the receiver; and therefore, a more reliable link can be expected. However, an implicit assumption to correct functionality of the protocol is that two nodes need to be in omni-directional range of each other. Similarly, a directional link establishment protocol that addresses the case where two nodes are only in directional-directional communication range of each other can be investigated.

A new Directional Medium Access Control (D-MAC) that is compatible with the current IEEE 802.15.3 MAC of WPAN for millimeter wave technology exploiting

directional antennas has been introduced. Moreover, a new directional neighbor discovery algorithm has been presented which does not require time synchronization or any location information of communicating nodes. The new D-MAC can still support devices that are not equipped with directional antennas. In other words, this D-MAC has legacy of the current IEEE 802.15.3 MAC. A directional MAC, without constraints of backward compatibility with the current IEEE 802.15.3 MAC, can be designed for possible new applications. For a piconet of DEVs that are all equipped with directional antennas, a better efficient MAC can be developed. Similarly, a D-MAC that addresses the case where two nodes are only in directional-directional communication range of each other can be investigated.

Bibliography

- [1] Q. H. Spencer, B. D. Jeffs, M. A. Jensen, A. L. Swindlehurst, “Modeling the statistical time and angle of arrival characteristics of an indoor multipath channel”, *IEEE Journal on Selected Areas in Communications*, Vol. 18, Issue 3, pp. 347 – 360, March 2000.
- [2] C. Chong, C. Tan, D. Laurenson, S. McLaughlin, M. A. Beach, A. R. Nix, “A New Statistical Wideband Spatio-Temporal Channel Model for 5-GHz Band WLAN Systems”, *IEEE Journal on Selected Areas in Communications*, Vol. 21, No. 2, pp. 139-150, Feb. 2003.
- [3] K. Huang, Z. Wang, “Millimeter Wave Circular Polarized Beam-Steering Antenna Array for Gigabit Wireless Communications”, *IEEE Trans. on Antennas and Propagation*, Vol. 54, pp. 743-746, Feb. 2006.
- [4] IEEE 802.15.3 – 2003, IEEE Standard for Information technology- Telecommunications and information exchange between systems- Local and metropolitan area networks- Specific requirements- Part 15.3: Wireless Medium Access Control (MAC) and Physical Layer (PHY) Specifications for High Rate Wireless Personal Area networks (WPANs).
- [5] S. J. Fortune, D. M. Gay, B. W. Kernighan, O. Landron, R. A. Valenzuela, M. H. Wright, “WISE design of indoor wireless systems: practical computation and optimization”, *IEEE Computational Science and Engineering*, Vol. 2, Issue: 1, pp. 58 – 68, Spring 1995.
- [6] D. W. Scott, “*Multivariate Density Estimation: Theory, Practice and Visualization*” New York: Wiley, 1992.

- [7] A. W. Bowman, A. Azzalini, “*Applied Smoothing Techniques for Data Analysis*”, Oxford University Press, 1997.
- [8] A. Saleh, R. A. Valenzuela, “A Statistical Model for Indoor Multipath Propagation”, *IEEE Journal on Selected Areas in Communications*, Vol. 5, Issue 2, pp. 128-137, Feb. 1987.
- [9] M. A. Hussein, “*Characterization of Ultra Wideband Communication Channels*”, Ph.D. Dissertation, Virginia Polytechnic Institute and State University, March 2003.
- [10] K. H. Li, M. A. Ingram, A. V. Nguyen, “Impact of clustering in statistical indoor propagation models on link capacity”, *IEEE Trans. on Communications*, Vol. 50, pp. 521-523, April 2002.
- [11] IEEE Std 802.11.b – 1999 (R2003), IEEE Standard for Information technology- Telecommunications and information exchange between systems- Local and metropolitan area networks- Specific requirements- Part 11: Wireless LAN Medium Access Control (MAC) and Physical Layer (PHY) Specifications: Higher-Speed Physical Layer Extension in the 2.4 GHz Band.
- [12] A. Mathew and Z. Lai, “Observations of the UMass Measurements,” IEEE 802.15.06-0137-00-003c, Denver, March 2006.
- [13] C. -C. Chong Y. E. Kim, S. K. Yong and S. S. Lee., “Statistical characterization of the UWB propagation channel in indoor residential environment,” *Wiley J. Wireless Communication Mobile Computing (Special Issue on UWB Communications)*, vol. 5 no. 5, pp. 503-512, Aug. 2005

- [14] H. B. Yang, M. H. A. J. Herben and P. F. M. Smulders, "Impact of Antenna Pattern and Reflective Environment on 60 GHz Indoor Radio Channel Characteristics", *IEEE Antennas and Wireless Propagation Letters*, Vol. 4, pp. 300-303, 2005.
- [15] S. Collonge, G. Zaharia and G. E. Zein, "Influence of the human activity on wideband characteristics of the 60GHz indoor radio channel," *IEEE Trans. Wireless Comm.* vol. 3, no. 6, pp. 2389-2406, Nov 2004.
- [16] G. D. Durgin, "*Space-time Wireless Channels*", Prentice Hall PTR, 2003.
- [17] J.A. Högbom, "Aperture synthesis with non-regular distribution of interferometer baselines", *Astronomy and Astrophysics*, Vol. 15, p. 417, 1974.
- [18] R. A. Valenzuela, O. Landron, D. L. Jacobs, "Estimating Local Mean Signal Strength of Indoor Multipath Propagation", *IEEE Transactions on Vehicular Technology*, Vol. 46, No.1, pp. 203-212, Feb. 1997.
- [19] Q. Spencer, M. Rice, B. Jeffs, and M. Jensen, "A statistical model for the angle of-arrival in indoor multipath propagation," in *Proc. IEEE Veh. Technol. Conf.*, pp. 1415–1419, 1997.
- [20] M. Toeltsch, J. Laurila, K. Kalliola, A. F. Molisch, P. Vainikainen, and E. Bonek, "Statistical characterization of urban spatial radio channels," *IEEE J. Select. Areas Commun.*, vol. 20, pp. 539–549, Apr. 2002.
- [21] J. E. Dietert and B. Rembold, "Stochastic channel model for outdoor applications based on raytrace simulations", in *Proc. of the Millennium Conf. on Antennas and Propagation (AP2000)*, Davos, Switzerland, Apr. 2000.
- [22] R. J. Cramer, R. A. Scholtz, and M. Z. Win, "Evaluation of an Ultra-Wide-Band Propagation Channel", *IEEE Transaction on Antennas and Propagation*, Vol. 50, No.

5, pp. 561-570, May 2002.

[23] D. Tse, P. Viswanath, “*Fundamentals of Wireless Communication*”, Cambridge University Press, 2005.

[24] K. Sayrafian, B. Neekzad, J. Perez, J. Baras “Ray-Tracing Simulation of the NICT Channel Measurements”, *IEEE Standard 802.15.3c mm-Wave channel modeling subgroup*, doc. # IEEE 802.15-06-0326-00-003c, July 2006.

[25] K. Sayrafian-pour, D. Kaspar, “Source-Assisted Direction Estimation Inside Buildings”, *Proceedings of the IEEE INFOCOM’06*, pp. 1-8, April 23-29, Barcelona, Spain , 2006.

[26] K. Sayrafian-Pour, D. Kspar, “Application of Beamforming in Wireless Location Estimation”, *EURASIP Journal on Applied Signal Processing*, Vol. 2006, Article ID 51673, 2006.

[27] T. S. Rappaport, “*Wireless Communications: Principles and Practice*”. Englewood Cliffs, NJ: Prentice-Hall, 1996.

[28] R. Ramanathan, “On the Performance of Ad Hoc Networks with Beamforming Antennas”, in *Proceedings of ACM MOBIHOC*, pp. 95-105, 2001.

[29] K. Huang, Z. Wang “Millimeter-Wave Circular Polarized Beam-Steering Antenna Array for Gigabit Wireless Communications” *IEEE Trans. on Antennas and Propagation*, Vol. 54, pp. 743-746, Feb 2006.

[30] H. Hashemi, “The Indoor Radio Propagation Channel”, *Proceedings of the IEEE*, Vol. 81, No. 7, pp. 943-968, July 1993.

- [31] R. B. Ertel, P. Cardieri, K. W. Sowerby, T. S. Rappaport, J. H. Reed, "Overview of spatial channel models for antenna array communication systems", *IEEE Personal Communications*, Vol. 5, Issue: 1, pp. 10–22, Feb. 1998.
- [32] Keshavarzian, E. Uysal-Biyikoglu, F. Herrman and A. Manjeshwar. "Energy-efficient link assessment in Wireless Sensor Networks", *Proc. of IEEE INFOCOM*, Vol. 3., pp. 1751-1761, Hong Kong, March 2004.
- [33] Y-B Ko, V. Shankarkumar and N.H. Vaidya, "Medium access control protocols using directional antennas in ad hoc networks", *IEEE INFOCOM*, pp 13-21, 2000.
- [34] M. McGlynn and S. Borbash. "Birthday protocols for low energy deployment and flexible neighbor discovery in ad hoc wireless networks" In *Proceedings of ACM MOBIHOC*, Long Beach, CA, pp. 137-145, 2001.
- [35] S. Vasudevan, J. Kurose, and D. Towsley, "On neighbor discovery in wireless networks with directional antennas," in *Proc. IEEE INFOCOM*, , vol. 4, pp. 2502–2512, 2005.
- [36] B. Neekzad, K. Sayrafian-Pour, J. S. Baras, "Energy Efficient Millimeter Wave Radio Link Establishment for Low Probability of Intercept with Smart Antenna", *proc. 25th Army Science Conference*, Orlando, FL, November 2006
- [37] B. Neekzad, K. Sayrafian-Pour, J. Perez, J. S. Baras, "Comparison of Ray Tracing Simulation and Millimeter Wave Channel Sounding Measurement", *in proc. 18th IEEE PIMRC*, pp. 1-5, Athens, Greece, September 2007
- [38] B. Neekzad, K. Sayrafian-Pour, J. Perez, J. S. Baras, "Clustering Characteristics of Millimeter Wave Indoor Channels", *in proc. IEEE WCNC*, Las Vegas, April 2008.